HHS Public Access

Author manuscript

Cell Rep. Author manuscript; available in PMC 2025 June 14.

Published in final edited form as:

Cell Rep. 2025 May 27; 44(5): 115694. doi:10.1016/j.celrep.2025.115694.

IRE1α promotes phagosomal calcium flux to enhance macrophage fungicidal activity

Michael J. McFadden[1], **Mack B. Reynolds**[1], **Britton C. Michmerhuizen**[1,5], **Einar B. Ólafsson**[1], **Sofia M. Marshall**[1], **Faith Anderson Davis**[1], **Tracey L. Schultz**[1], **Takao Iwawaki**[2], **Jonathan Z. Sexton**[3,4], **Mary X.D. O'Riordan**[1,*], **Teresa R. O'Meara**[1,6,*]

[1]Department of Microbiology and Immunology, University of Michigan, Ann Arbor, MI 48109, USA

[2]Department of Life Science, Medical Research Institute, Kanazawa Medical University, Ishikawa 920-0293, Japan

[3]Department of Internal Medicine, Division of Gastroenterology, University of Michigan Medical School, Ann Arbor, MI 48109, USA

[4]Department of Medicinal Chemistry, College of Pharmacy, University of Michigan, Ann Arbor, MI 48109, USA

[5]Present address: College of Human Medicine, Michigan State University, Grand Rapids, MI 49503, USA

[6]Lead contact

SUMMARY

The mammalian endoplasmic reticulum (ER) stress sensor inositol-requiring enzyme 1α (IRE1α) is essential for cellular homeostasis and plays key roles in infection responses, including innate immunity and microbicidal activity. While IRE1α functions through the IRE1α-XBP1S axis are known, its XBP1S-independent roles are less well understood, and its functions during fungal

*Correspondence: oriordan@umich.edu (M.X.D.O.), tromeara@umich.edu (T.R.O.).

AUTHOR CONTRIBUTIONS

Conceptualization: M.J.M., M.X.D.O., and T.R.O. Investigation: M.J.M., M.B.R., B.C.M., E.B.O., S.M.M., F.A.D., and T.L.S. Formal analysis: M.J.M., T.R.O., and M.X.D.O. Software: M.J.M., M.B.R., B.C.M, E.B.O., and T.R.O. Writing – original draft: M.J.M., T.R.O., and M.X.D.O. Writing – review & editing: M.J.M., M.B.R., B.C.M., E.B.O., S.M.M., F.A.D., T.L.S., M.X.D.O., and T.R.O. Funding acquisition: M.J.M., M.X.D.O., and T.R.O.

RESOURCE AVAILABILITY

Lead contact

Further information and requests for resources and reagents should be directed to and will be fulfilled by the lead contact, Teresa O'Meara (tromeara@umich.edu).

Materials availability

All unique/stable reagents generated in this study are available from the lead contacts with a completed materials transfer agreement.

Data and code availability

- Data: All raw data related to RNA-seq are available through GEO (accession no.: GSE244303).
- Code: CellProfiler pipelines for image quantification are available in Data S1. Software for cellular calcium flux analysis are available from GitHub (https://github.com/EinarOlafsson/spacr).
- Other items: All raw data related to microscopy are available upon request.

DECLARATION OF INTERESTS

The authors declare no competing interests.

infection are still emerging. We demonstrate that *Candida albicans* activates macrophage IRE1α via C-type lectin receptor signaling independent of protein misfolding, suggesting non-canonical activation. IRE1α enhances macrophage fungicidal activity by promoting phagosome maturation, which is crucial for containing *C. albicans* hyphae. IRE1α facilitates early phagosomal calcium flux post-phagocytosis, which is required for phagolysosomal fusion. In macrophages lacking the IRE1α endoribonuclease domain, defective calcium flux correlates with fewer ER-early endosome contact sites, suggesting a homeostatic role for IRE1α-promoting membrane contact sites. Overall, our findings illustrate non-canonical IRE1α activation during infection and a function for IRE1α in supporting organelle contact sites to safeguard against rapidly growing microbes.

Graphical Abstract

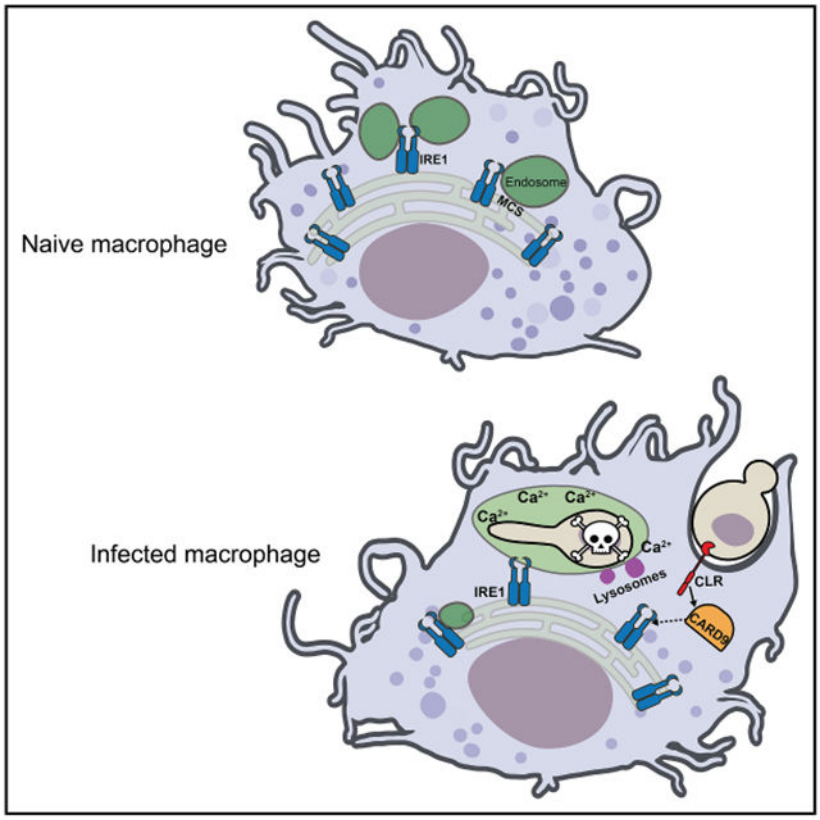

In brief

McFadden et al. find the endoplasmic reticulum (ER) stress sensor inositol-requiring enzyme 1α (IRE1α) is activated by C-type lectin receptor signaling during *Candida albicans* infection without protein misfolding. IRE1α enhances calcium flux at the *C. albicans*-containing phagosome, likely through coordinating ER-phagosome contact sites. IRE1α promotes phagosome maturation and integrity, as well as macrophage fungicidal activity.

INTRODUCTION

Intracellular infection by pathogens triggers cell stress programs, including the unfolded protein response (UPR), whose three branches (inositol-requiring enzyme 1α [IRE1α], protein kinase RNA-like endoplasmic reticulum kinase, and activating transcription factor 6 [ATF6]) have broad consequences for host defenses through the regulation of innate immunity, cellular metabolism and homeostasis, and cell differentiation or death pathways.[1-4] Canonically, accumulation of misfolded proteins in the endoplasmic reticulum (ER) lumen triggers activation of the UPR, which then restores cellular homeostasis by modulating gene expression to promote protein folding and ER expansion.[5] After detecting misfolded proteins, IRE1α assembles into small oligomers that allow for *trans*-autophosphorylation and activation of its endonuclease domain to perform non-canonical mRNA splicing of *Xbp1*.[6-9] *Xbp1* splicing is required for translation and protein synthesis of the transcription factor XBP1S, which promotes the transcription of genes involved in ER quality control.[10] Additionally, the regulatory roles of IRE1α extend beyond XBP1S, as IRE1α itself can modulate JNK pathway activation, orchestrate organelle contact sites, and regulate metabolic plasticity.[11-14] However, the IRE1α branch of the UPR can also be selectively triggered by infection or detection of microbe-associated molecular patterns by pattern recognition receptors (PRRs), such as Toll-like receptors (TLRs).[15,16] Through the IRE1α-XBP1S axis, the cell can promote the expression of proinflammatory cytokines[15,17] and modulate metabolic plasticity[18] and ER homeostasis[19] during infection. Additionally, IRE1α can facilitate intra-organelle communication for ER-mitochondria calcium signaling and reactive oxygen species (ROS) generation.[13,20,21] Through these regulatory effects on gene expression, metabolism, and redox balance, IRE1α can promote bacterial killing or inflammasome activation in phagocytic cells.[20,22] However, despite these known roles of IRE1α in bacterial and viral infection, mechanistic understanding of how IRE1α functions during fungal infection is limited.

Given its many functions in host responses to infection, we investigated the role of IRE1α in macrophage interactions with *Candida albicans,* a common fungus in the human mucosal microbiota and an opportunistic pathogen.[23] Recent work found that IRE1α is activated in neutrophils upon *C. albicans* infection and contributes to immunopathology in systemic disease.[24] However, the function of IRE1α in macrophage responses to *C. albicans* infection remained unclear. Macrophages are crucial for early antifungal responses *in vivo* and may control *C. albicans* dissemination through recognition and subsequent fungicidal activity and cytokine signaling to recruit neutrophils to sites of infection.[25-27] During intracellular growth in macrophages, *C. albicans* hyphal formation can mediate phagosomal escape and macrophage killing through lysis or pyroptosis.[28-33] Recent work reported that lysosome fusion with the expanding *C. albicans*-containing phagosome is crucial to maintain phagosome integrity and fungicidal activity,[34-37] suggesting that phagosome maturation is critical for the macrophage antifungal response, although the full suite of macrophage microbicidal functions are not clear.

Here, we report that IRE1α activation during infection in macrophages can be triggered through the C-type lectin receptor (CLR) signaling pathway independently of protein misfolding. IRE1α supports macrophage fungicidal activity *in vitro* and *in vivo* through

promoting phagosome maturation. Mechanistically, IRE1α enhances early phagosomal calcium, which is required for downstream lysosome recruitment to the *C. albicans* phagosome. Failure to undergo phagosomal calcium flux in macrophages lacking the IRE1α endoribonuclease domain correlated with deficient contact sites between the endosomal network and the ER at resting state. We propose that the homeostatic function of IRE1α in coordinating ER-endosome contact sites equips macrophages for efficient phagosome maturation to contain rapidly growing pathogens.

RESULTS

C. albicans infection results in the activation of macrophage IRE1α

During systemic *C. albicans* infection, phagocytic cells can phagocytose and kill *C. albicans* to stymie its spread. To evaluate the role of IRE1α in anti-fungal responses, we first determined whether macrophage IRE1α is activated during *C. albicans* infection by measuring splicing of *Xbp1* mRNA in immortalized bone marrow-derived macrophages (iBMDMs) infected with *C. albicans* or treated with bacterial lipopolysaccha-ride (LPS) or thapsigargin, as positive controls. *C. albicans* infection induces *Xbp1* splicing in wild-type (WT) iBMDM, albeit to a lesser extent than the positive controls LPS and thapsigargin (Figure 1A). *Xbp1* splicing did not occur in response to any of the treatments in a clonal iBMDM cell line lacking exons 20 and 21 of IRE1α (IRE1$^{\Delta R}$), which are required for endonuclease activity[38] (Figures 1A and 1B). Analysis of *Xbp1* splicing by RT-qPCR over time showed induction of *Xbp1-S* at 4 h post-infection (hpi) with *C. albicans* (Figure 1C). As the SC5314 reference strain can be an outlier in virulence and hyphal formation,[23,39] we measured *Xbp1-S* induction following infection with commensal *C. albicans* isolates from healthy donors,[23] including those that do not form robust hyphae during macrophage infection. All *C. albicans* isolates resulted in comparable macrophage *Xbp1* splicing to SC5314 (Figure 1D), suggesting that *Xbp1-S* formation does not depend on virulence or hyphal formation. *Xbp1* splicing enables translation of the transcription factor XBP1S to induce the transcription of ER quality control-responsive genes following unfolded protein stress. However, while LPS and thapsigargin treatment led to accumulation of XBP1S by 4 hpi, infection with *C. albicans* did not lead to the induction of XBP1S protein (Figures S1A and S1B). Thus, IRE1α function during *C. albicans* infection of macrophages is likely independent of the transcription factor XBP1S or canonical functions of IRE1α in the UPR.

CLR signaling drives TRAF6-independent IRE1α activation during *C. albicans* infection

CLRs, which detect cell wall components of *C. albicans*,[40] are the major PRR for *C. albicans* recognition in macrophages.[41] To determine whether CLR signaling contributes to IRE1α activation during infection, we measured *Xbp1* splicing in iBMDM lacking CLR signaling adaptor protein CARD9 (CARD9 knockout [KO]) (Figure S1C). CARD9 was required for *Xbp1* splicing in response to *C. albicans* but dispensable for the response to LPS, which activates IRE1α through TLR4[42,43] (Figure 1E). We also observed CARD9-dependent *Xbp1* splicing in response to *C. albicans* infection in primary BMDM (Figures S1C and S1D). These results suggest that CLR signaling is required for IRE1α activation in response to *C. albicans*. Next, we addressed whether CLR agonism is sufficient to stimulate IRE1α activity by treating WT or IRE1$^{\Delta R}$ iBMDM with a Dectin-1 specific agonist,

depleted zymosan (d-zymosan). d-Zymosan was sufficient to trigger IRE1α-dependent *Xbp1* splicing (Figure 1F). Like *C. albicans* infection, *Xbp1* processing by IRE1α was more strongly stimulated by LPS than by d-zymosan (Figure 1F).

We next investigated whether TLRs contribute to IRE1α activation in response to *C. albicans* by measuring *Xbp1* splicing in BMDM lacking TLR2, TLR4, and TLR9 (TLR2/4/9 KO) and found comparable *Xbp1* splicing to WT iBMDM in response to *C. albicans* and d-zymosan (Figure 1G). As expected, *Xbp1* splicing was ablated in response to LPS (Figure 1G). These results demonstrate that CLR signaling is necessary and sufficient for IRE1α activation in response to *C. albicans*.

We next tested whether TLR and CLR signaling use the same signaling mediators to activate IRE1α. TRAF6 is a crucial E3 ubiquitin ligase involved in innate immune signaling for both TLR and CLR pathways[44,45] and can directly ubiquitinate IRE1α after LPS treatment,[15,16] although its role in IRE1α activation during fungal infection is unknown. Therefore, we tested whether TRAF6 is involved in IRE1α activation in response to *C. albicans* infection. While KO of TRAF6 (Figure S1E) resulted in the expected decrease in *Xbp1* splicing in response to LPS, *Xbp1* splicing in response to *C. albicans* was not affected (Figure 1H). These data reveal that CLR signaling through CARD9 triggers IRE1α activation independently of TLR signaling or TRAF6, in contrast to LPS-driven IRE1α activation, demonstrating that *C. albicans* activates IRE1α in macrophages through a mechanism distinct from bacterial ligands.

PRR-mediated activation of IRE1α occurs independently of misfolded protein stress

A potential mechanism for CLR-mediated IRE1α activation could be through overwhelming the protein folding capacity of the ER due to increased cytokine production, leading to protein misfolding and UPR activation. Therefore, we inhibited transcription or translation during infection with *C. albicans*. While the inhibition of transcription and translation, with actinomycin D or cycloheximide, respectively, decreased *Xbp1* transcript abundance (Figures S2A and S2B), neither treatment inhibited *Xbp1* splicing during *C. albicans* infection (Figures 2A, 2B, S2A, and S2B). These data indicate that new gene synthesis does not contribute to IRE1α activation during *C. albicans* infection and suggest that *C. albicans* infection does not induce unfolded proteins. To measure this directly, we used the dye thioflavin T (ThT), which exhibits increased fluorescence in the presence of misfolded proteins.[46] While ThT intensity showed an expected increase at 2 h post-thapsigargin treatment, neither *C. albicans* infection nor LPS increased ThT intensity over mock (Figures 2C and 2D). Furthermore, neither *C. albicans* infection nor LPS treatment led to increased ThT intensity at 4 hpi, suggesting IRE1α activation occurs without accumulation of misfolded proteins during these responses (Figure 2E). Even at 8 hpi, *C. albicans* infection did not induce protein misfolding, while LPS treatment did (Figure 2F), although well after the robust IRE1α activation at 4 h (Figure 1A). Similar results were observed in primary BMDM, where only thapsigargin treatment led to significantly increased ThT intensity (Figures S2C-S2E).

These data suggested that infection may not result in a global UPR response and that IRE1α is selectively activated during *C. albicans* infection, further supporting protein-misfolding-

independent activation of IRE1α. To further test this hypothesis, we measured induction of canonical UPR-responsive genes by RT-qPCR (Figures 2G and 2H). Infection with *C. albicans* or treatment with d-zymosan did not induce UPR-responsive genes (*Ddit3*, *Grp78*, *Grp94*, and *Xbp1-T*) at 4 or 6 h. Similarly, LPS did not lead to global induction of UPR-responsive genes, and only significantly induced *Grp78* at 4 h and *Xbp1-T* at 6 h. Conversely, thapsigargin triggered induction of all these genes at 4 and 6 h post-treatment (Figures 2G and 2H). Similar results were observed in primary BMDM (Figures S2F and S2G). Beyond UPR gene expression induction, immunoblotting to measure additional UPR-associated signaling, such as ATF6 cleavage, eukaryotic initiation factor-2α (eIF2α) phosphorylation, ATF4 expression, and accumulation of K48-linked poly-ubiquitylated proteins, revealed that *C. albicans* infection does not induce characteristic UPR signatures (Figure S3), consistent with a lack of global UPR and infection-specific stimulation of IRE1α. Thapsigargin treatment triggered ATF6 cleavage, eIF2α phosphorylation, and ATF4 expression, and MG-132 treatment also triggered eIF2α phosphorylation and ATF4 expression and accumulation of K48-ubiquitylated proteins, as expected (Figure S3). Together, these results highlight that protein misfolding is not required for IRE1α activation during innate immune responses and points to a non-canonical mode of IRE1α activation during infection.

IRE1α promotes macrophage fungicidal activity

We next explored the impact of IRE1α on macrophage antifungal capacity. The mechanisms by which macrophages kill *C. albicans* are not well understood, and microbicidal effectors like ROS are not reliable predictors of macrophage fungicidal activity.[47,34] We measured the ability of IRE1α WT and IRE1$^{\Delta R}$ macrophages to kill phagocytosed *C. albicans* using a dual fluorescence assay in which near-infrared fluorescent protein (iRFP)-expressing *C. albicans* is pre-labeled with calcofluor white (CFW) prior to macrophage infection (Figure 3A). Live *C. albicans* express iRFP and are CFW labeled (iRFP^{+} CFW^{+}), while killed *C. albicans* lose iRFP fluorescence (iRFP^{-} CFW^{+}) (Figure S4A). Using this assay, we observed that IRE1$^{\Delta R}$ macrophages were defective at killing phagocytosed *C. albicans*, demonstrating that IRE1α contributes to the fungicidal activity of macrophages (Figure 3B). To better understand how IRE1α influences *C. albicans* killing, we turned to pharmacological inhibitors. MKC8866 binds within the active site of the IRE1α endoribonuclease domain, inhibiting RNase activity,[48] while KIRA8 binds to the ATP binding site, inhibiting IRE1α dimerization, kinase activity, and RNase activity.[49,50] Both inhibitors reduced IRE1α RNase activity, as measured by *Xbp1* splicing in mock- or thapsigargin-treated cells (Figure S4B). Pretreatment with MKC8866 did not reduce the fungicidal activity of macrophages, suggesting that IRE1α RNase activity is not necessary for fungal killing (Figure 3C). However, treatment with KIRA8 led to a similar decrease in fungicidal activity as seen in IRE1$^{\Delta R}$ macrophages. Notably, deletion of exons 20 and 21 of IRE1α may impair more than RNase activity, as previous reports showed decreased expression and kinase activity resulting from this truncation.[51,52] Neither MKC8866 nor KIRA8 had any additional impact on the fungicidal activity of IRE1$^{\Delta R}$ macrophages (Figure 3C). Therefore, the fungicidal activity of macrophages is augmented by the dimerization status of IRE1α or its kinase activity.

To examine the impact of IRE1α during *C. albicans* infection in a murine model, we conditionally deleted IRE1α in macrophages and neutrophils ($IRE1^{fl/fl}$ $LysM^{Cre}$), followed by systemic infection of mice with *C. albicans* expressing iRFP. Previous work demonstrated that the IRE1α-XBP1S axis in neutrophils drives fatal renal immunopathology starting at 5 days post-systemic *C. albicans* infection.[24] However, we found that female $IRE1^{fl/fl}LysM^{Cre}$ mice had higher levels of serum cytokines, such as tumor necrosis factor (TNF) and interleukin-6 (IL-6), than littermate controls ($IRE1^{fl/fl}$) at 24 hpi (Figure S4C). Increased cytokine levels were observed specifically in infected $IRE1^{fl/fl}LysM^{Cre}$ female mice, but not infected $IRE1^{fl/fl}LysM^{Cre}$ male mice (Figure S4D), suggesting sex-specific roles for IRE1α during early *C. albicans* infection. Additionally, we determined whether IRE1α supports the fungicidal activity of phagocytes *in vivo* using an immunofluorescence assay with dissociated kidney samples from $IRE1^{fl/fl}LysM^{Cre}$ mice compared to $IRE1^{fl/fl}$ controls, as kidneys are the primary target organ during systemic *C. albicans* infection. For this assay, *C. albicans* viability in kidney-associated myeloid cells was measured using an anti-*Candida* antibody to identify total *C. albicans* and iRFP to indicate viability, as well as anti-CD11b to identify leukocytes that had phagocytosed *C. albicans* (Figure 3D). While overall *C. albicans* viability in the kidney tissue was not different between $IRE1^{fl/fl}LysM^{Cre}$ mice and $IRE1^{fl/fl}$ control mice (Figure 3E), *C. albicans* killing by phagocytic cells was less effective in mice lacking IRE1α activity (Figure 3F). These data suggest that IRE1α supports the fungicidal activity of phagocytic cells *in vivo*, in agreement with our *in vitro* data, and suggest a sex-specific role for IRE1α in coordinating cytokine responses in female mice.

IRE1α promotes phagosome maturation during *C. albicans* infection

We next tested potential mechanisms by which IRE1α could potentiate fungal killing. We first measured the ability of IRE1 WT and $IRE1^{\Delta R}$ macrophages to phagocytose *C. albicans*. After phagocytosis by macrophages, external *C. albicans* was stained with an anti-*Candida* antibody prior to permeabilization, and CFW was used to stain both internal and external *C. albicans* after permeabilization (internal *C. albicans* CFW^+, external *C. albicans* CFW^+FITC^+). $IRE1^{\Delta R}$ macrophages showed increased phagocytosis of *C. albicans* (Figures S5A and S5B), ruling out a phagocytosis defect as the basis for defective fungicidal activity. Following uptake of large particles, the ER regulates phagosome maturation, albeit through poorly understood mechanisms.[53] Importantly, phagosome maturation is required for containment of *C. albicans* hyphae within the phagosome, as lysosome fusion allows membrane donation to support phagosome expansion.[35] Therefore, we tested whether $IRE1^{\Delta R}$ macrophages showed impaired phagosome maturation during *C. albicans* infection by measuring the recruitment of the lysosomal protein LAMP1 to the *C. albicans* phagosome (Figures 4A and 4B). WT macrophages recruited LAMP1 to the phagosome by 2 hpi, but $IRE1^{\Delta R}$ failed to efficiently recruit LAMP1 to the *C. albicans*-containing phagosome (Figures 4A and 4B). Overall, lysosome biogenesis was unimpaired in $IRE1^{\Delta R}$ macrophages, as LysoSensor Blue/Yellow dye showed that $IRE1^{\Delta R}$ macrophages had acidity similar to that of IRE1 WT macrophages, and *C. albicans* infection or ammonium chloride treatment led to alkalinization of both cell lines (Figure S5C).[36,54-56] Similar results were observed using microscopy to measure fluorescence intensity of LysoTracker, which labels acidic compartments (Figures S5D and S5E). These data suggest that IRE1α is required for efficient phagolysosomal fusion during *C. albicans* infection.

To determine whether failure to recruit lysosomes to the phagosome underlies the fungicidal defect observed in IRE1$^{\Delta R}$ macrophages, we tested the effect of bafilomycin A (BafA), which inhibits vacuolar ATPase activity and thus phagosome-lysosome fusion (Figure S5F), on the ability of IRE1 WT and IRE1$^{\Delta R}$ macrophages to kill *C. albicans* (Figure 4C). BafA treatment suppressed the fungicidal activity of both IRE1 WT and IRE1$^{\Delta R}$ macrophages, reinforcing the importance of phagolysosomal fusion for the killing of *C. albicans*. Additionally, BafA treatment ablated the difference between IRE1 WT and IRE1$^{\Delta R}$ macrophages in fungicidal capacity, demonstrating that defective phagolysosomal fusion in IRE1$^{\Delta R}$ macrophages is responsible for compromised *C. albicans* killing (Figure 4C).

IRE1α promotes phagosome integrity and macrophage fungistatic activity

As lysosome recruitment maintains the integrity of the expanding phagosome during *C. albicans* infection,[35] we reasoned that *C. albicans* may escape the phagosome more readily in IRE1$^{\Delta R}$ macrophages. To test this, we used a pulse-chase assay to measure phagosome leakage, in which endosomes are pre-labeled with sulforhodamine B (SRB), allowing fusion with *C. albicans*-containing phagosomes and monitoring of phagosome rupture (Figure 4D).[35,57] Imaging the *C. albicans*-containing phagosome over time revealed that SRB was lost from the phagosome more rapidly in IRE1$^{\Delta R}$ macrophages, supporting the hypothesis that IRE1α acts to maintain the integrity of the *C. albicans*-containing phagosome (Figure 4E). As the phagolysosomal environment restricts *C. albicans* hyphal growth,[58] we measured hyphae over time in WT and IRE1$^{\Delta R}$ macrophages and found that *C. albicans* hyphal growth is increased at 4 hpi in IRE1$^{\Delta R}$ macrophages (Figure S6A), demonstrating that IRE1α promotes macrophage fungistatic activity. Phagosome rupture during *C. albicans* infection has been associated with macrophage proinflammatory cytokine production.[29,32,35,59] Therefore, we tested the secretion of IL-1β, TNF, and IL-6 from WT and IRE1$^{\Delta R}$ macrophages after LPS treatment to transcriptionally prime the NLRP3 inflammasome components, followed by *C. albicans* infection (Figures S6B-S6D). Consistent with increased phagosome rupture observed in IRE1$^{\Delta R}$ macrophages, we also saw increased supernatant IL-1β and TNF levels, while IL-6 levels were unaffected (Figures S6B-S6D). Together, these data support a model in which IRE1α supports phagolysosomal fusion during *C. albicans* infection of macrophages to maintain phagosome integrity and promote killing of ingested *C. albicans*.

IRE1α promotes phagosomal calcium flux necessary for phagosome maturation

To explore the role of IRE1α in phagosome maturation, we investigated its impact on gene expression during *C. albicans* infection or mock treatment using RNA sequencing (RNA-seq). Gene Ontology enrichment analysis revealed that genes involved in endocytosis and calcium homeostasis were enriched among downregulated genes in IRE1$^{\Delta R}$ macrophages (Table S1, 1.2). These included genes involved in ER homeostasis (*Kctd17*, *Atp2a3*, *Gramd2*),[60-62] as well as the major lysosome calcium channels *Mcoln1* and *Mcoln3*[63] (Figure S7F). However, the expression of genes involved in general cellular calcium uptake and homeostasis, such as *Calm1*, *Calr*, *Stim1*, *Orai1-3*, and *Ryr1* and *Ryr3*, was similar in WT and IRE1$^{\Delta R}$ macrophages (Figure S7F). Therefore, we hypothesized that organellar calcium signaling may be impaired in IRE1$^{\Delta R}$ macrophages.

Calcium flux regulates phagosome formation and maturation[64] and is required for lysosome recruitment to the phagosome during *C. albicans* infection.[35] We investigated whether calcium flux is perturbed in IRE1$^{\Delta R}$ macrophages during phagocytosis of *C. albicans* using the fluorescent calcium ion indicator Fluo4-AM. In WT macrophages, calcium flux was observed during macrophage-*C. albicans* interactions and during phagocytosis of *C. albicans* (Figure S8A; Video S1). At baseline, WT and IRE1$^{\Delta R}$ macrophages showed similar Fluo4 fluorescence intensity, suggesting that overall calcium stores are not depleted (Figure S8B). Cellular calcium flux was comparable between WT and IRE1$^{\Delta R}$ macrophages, as similar frequency of cellular calcium flux was observed (Figures S8C and S8D), as well as similar "excitability" of macrophages during *C. albicans* infection (Figure S8E). However, shortly after phagocytosis, phagosomal calcium influx was frequently observed in WT macrophages (Figure 5A; Video S1), seen as a clear but transient ring around the engulfed yeast. In contrast, phagosomal calcium flux was rarely observed in IRE1$^{\Delta R}$ macrophages after phagocytosis of *C. albicans* (Figure 5A; Video S2). Quantification of phagosomal calcium flux at 20 min post-infection in WT macrophages revealed that roughly half of macrophages that phagocytosed *C. albicans* had active phagosomal calcium flux, whereas fewer than 20% of IRE1$^{\Delta R}$ macrophages showed phagosomal calcium flux (Figure 5B). Additionally, the fluorescence intensity of the *C. albicans* phagosome relative to the cytosol was higher in WT macrophages than in IRE1$^{\Delta R}$ macrophages (Figure 5C). Together, these data suggest that phagosomal calcium flux is specifically impaired in IRE1$^{\Delta R}$ macrophages.

Phagosome-derived calcium is required for lysosome recruitment during *C. albicans* infection, and calcium chelation disrupts phagosome maturation.[35] To test the hypothesis that calcium flux is required for maturation of *C. albicans*-containing phagosomes, we treated macrophages with a cell-permeable calcium chelator, BAPTA-AM, during *C. albicans* infection. BAPTA-AM impaired phagosome maturation in WT macrophages, while defective phagosome maturation observed in IRE1$^{\Delta R}$ macrophages was not further impacted (Figure 5D). These results suggest that defective phagosomal calcium flux in IRE1$^{\Delta R}$ macrophages perturbs phagosome maturation. Depletion of ER calcium stores with thapsigargin prior to infection enhanced phagosomal calcium flux in both WT and IRE1$^{\Delta R}$ macrophages (Figures S9A and S9B), consistent with prior reports.[65] Thapsigargin treatment induces oligomerization and kinase activity of IRE1α, and enhancement of these functions of IRE1α may also be involved in mediating phagosomal calcium flux, in agreement with these functions of IRE1α supporting fungicidal activity (Figure 3C). Our data support a model in which IRE1α promotes early phagosomal calcium flux during *C. albicans* infection, allowing phagosome maturation and fungal killing.

To evaluate specificity for phagocytosed cargo in triggering phagosomal calcium flux, we incubated Fluo4-stained macrophages with polystyrene fluorospheres, which were phagocytosed but did not trigger phagosomal calcium flux (Figure S10A). Additionally, methicillin-resistant *Staphylococcus aureus* infection triggered phagosomal calcium flux, although this process occurred independently of IRE1α activity (Figures S10B and S10C). Finally, to test whether *C. albicans* uptake could trigger phagosomal calcium flux within the fluorosphere phagosome in *trans*, we co-incubated Fluo4-stained macrophages with *C. albicans* and fluorospheres. We only observed calcium flux within the *C. albicans*-containing phagosome; fluorosphere phagosomes did not undergo observable calcium flux, even in

macrophages containing both *C. albicans* and fluorospheres (Figure S10D). These data demonstrate that phagocytosis is not sufficient to trigger phagosomal calcium flux, although both bacterial and fungal pathogens can activate this process. Furthermore, the role of IRE1α in coordinating phagosomal calcium flux appears to be unique to *C. albicans* among our tested phagocytic cargo, suggesting potential specificity for IRE1α in regulating CLR-triggered phagosomal calcium flux.

IRE1α promotes contact sites between the ER and endosomal network

The ability of IRE1α to promote early phagosomal calcium flux within 20 min of infection with *C. albicans* suggested that this function of IRE1α likely precedes its activation during infection. IRE1α can promote contact sites between ER and mitochondria, thus influencing calcium signaling between these organelles.[13] We hypothesized that IRE1α may promote contact sites between the ER and endosomal network, promoting calcium flux in the phagosome early after phagocytosis. To test this, we used the proximity ligation assay (PLA) to probe sites of proximity between the ER and early endosomes. We employed antibodies marking the ER (anti-KDEL) and early endosomes (anti-EEA1) and quantified the number of PLA puncta per macrophage to measure ER-endosome contact sites. Strikingly, these contact sites were depleted in IRE1$^{\Delta R}$ macrophages both at basal state and during *C. albicans* infection (Figures 5E and 5F). These data suggest that IRE1α promotes contact sites between the ER and early endosomes or phagosomes in macrophages, supporting a model in which IRE1α promotes calcium signaling between these organelles and allows subsequent lysosome fusion to drive phagosome maturation. Furthermore, as this function of IRE1α in promoting ER-phagosome contact sites likely has downstream consequences for phagosome maturation, this homeostatic function of IRE1α may safeguard against infection by rapidly proliferating pathogens.

DISCUSSION

Here, we show that macrophages lacking IRE1α activity have impaired fungicidal capacity due to inefficient lysosome recruitment to the *C. albicans* phagosome, allowing phagosomal escape by *C. albicans* and evasion of fungicidal effectors. IRE1α promotes phagosomal calcium flux, which is correlated with the ability of IRE1α to promote homeostatic contact sites between endosomes and the ER membrane. These results reveal a role for IRE1α in regulating the endocytic pathway and propose a model in which basal functions of IRE1α support the maturation and integrity of the phagosome during infection with a rapidly growing pathogen.

We found that *C. albicans* selectively activates IRE1α through the CLR signaling pathway without a requirement for protein misfolding. Proactive (or protein-misfolding-independent) activation of the UPR or its individual branches during certain physiological stimuli has been proposed and discussed previously.[66] However, direct evidence of protein-misfolding-independent IRE1α activation and the mechanisms driving it remained elusive. A potential route of IRE1α activation is post-translational modification, such as ubiquitination or phosphorylation.[16,67] Ubiquitination of IRE1α by the E3 ubiquitin ligases TRAF6 and CHIP occurs in response to LPS treatment or geldanamycin-induced ER

stress, respectively.[16,68] However, IRE1α activation was TRAF6 independent during *C. albicans* infection, suggesting an alternative mechanism of activation. CLR-mediated IRE1α activation required CARD9 in response to *C. albicans*, potentially facilitating interaction of IRE1α with a post-translational modifier to enable its activation.

When investigating the consequences of IRE1α activity during antifungal responses, we found a regulatory function of IRE1α in promoting transient phagosomal calcium flux. Interestingly, as IRE1α-dependent phagosomal calcium flux was observed within minutes of infection, this phenotype may reflect basal functions of IRE1α. Indeed, IRE1α promoted endosome-ER contact sites in macrophages at resting state, prior to *C. albicans* infection. These membrane contact sites affect endosome maturation, although their regulatory functions are still emerging.[53,69] While calcium flux is required for phagosome maturation during *C. albicans* infection,[35] the transient accumulation of calcium at the *C. albicans* phagosome had not been described previously, although a similar process had been observed during *Aspergillus fumigatus* infection.[70] Our use of pharmacological inhibitors allowed us to determine that IRE1α dimerization or kinase activity is likely involved in coordinating ER-endosome/phagosome contact sites. IRE1α exists as a homodimer at resting state,[9] which may influence its structural roles at membrane contact sites. Understanding the structural requirements for homeostatic functions of IRE1α will be crucial to understand its basal functions.

IRE1α in the myeloid compartment drives immunopathology during systemic *C. albicans* infection, and IRE1α ablation in neutrophils prolonged survival of infected hosts in a murine systemic *C. albicans* infection model.[24] This work showed that ROS production in *C. albicans*-infected neutrophils triggers protein misfolding and IRE1α activation, and subsequent XBP1S production enhances the production of proinflammatory cytokines, driving fatal kidney immunopathology.[24] Our work complements these findings, uncovering functions of IRE1α in macrophage anti-fungal responses during early stages of infection. We similarly found that stimulation of the CLR pathway can trigger IRE1α activation, although protein misfolding is not required for early IRE1α activation in macrophages, and we did not observe notable increases in XBP1S expression during *C. albicans* infection in macrophages. Additionally, while IRE1α was not required for neutrophil fungicidal activity, we found that it does support macrophage fungicidal activity, which may protect macrophage viability to allow for pro-inflammatory cytokine secretion.

In summary, our work suggests that innate immune signaling can trigger non-canonical activation of IRE1α and highlights roles for IRE1α in the fungicidal capacity of macrophages. These findings will help shape our understanding of the activation and function of IRE1α in infection and other settings. Protein-misfolding-independent activation of IRE1α suggests new paradigms to explore in other contexts, such as sterile inflammation and obesity,[71] and a critical role for IRE1α as a sensor of other agents that may perturb cellular homeostasis. Dissection of the molecular mechanisms regulating early IRE1α activation may identify new therapeutic targets for the regulation of IRE1α activity. Furthermore, a better understanding of the role of IRE1α in the endocytic pathway will provide fundamental understanding of communication between the ER and endocytic compartments. Overall, these findings reveal exciting roles for IRE1α in coordinating the

maturation of the phagocytic pathway during fungal infection with broad potential impacts for our understanding of cell biology.

Limitations of the study

We demonstrate that IRE1α is non-canonically activated by CLR signaling through CARD9, although full mechanistic understanding of how CLR signaling triggers IRE1α activation remains unresolved. Our data suggest that IRE1α promotes phagosomal calcium flux to augment phagosome maturation, allowing macrophages to contain and kill *C. albicans*. However, future work will be required to test whether restoration of phagosomal calcium flux rescues phagosome maturation and fungicidal activity in IRE1$^{\Delta R}$ macrophages. Additionally, while we show that IRE1α promotes macrophage fungicidal activity *in vitro* and *in vivo*, it is unclear whether this function of macrophage IRE1α is important for host survival during systemic infection, as the LysM-Cre promoter targets both macrophages and neutrophils.[72] Therefore, it is difficult to differentiate between macrophage fungicidal activity and the previously discovered role of neutrophil IRE1α in immunopathology.[24]

STAR★METHODS

EXPERIMENTAL MODELS AND STUDY PARTICIPANT DETAILS

Cell lines: All cell lines were incubated at 37°C with 5% CO_2. Bone marrow-derived macrophages (BMDM) were grown in bone marrow media (BMM), containing modification of Eagle's medium (DMEM; Thermo Fisher Scientific) supplemented with 20% fetal bovine serum (Thermo Fisher Scientific), 30% L929 conditioned media, and 1 mM sodium pyruvate (Thermo Fisher Scientific). BMDM were immortalized (iBMDM) using J2 retrovirus.[81] L-929 cells were cultured in minimum essential Eagle's medium supplemented with 2 mM L-glutamine, 1 mM sodium pyruvate, 1 mM nonessential amino acid, 10 mM HEPES, and 10% FBS. All experiments were performed in experimental media (RPMI supplemented with 3% FBS) unless otherwise indicated. All cell lines were verified as mycoplasma free using the Lookout Mycoplasma PCR Detection Kit (Sigma-Aldrich) and genetic identities were validated by PCR, western blotting, or functional assays. IRE1$^{fl/fl\ exon20\text{-}21}$ (−/+ Cre) mice were a gift from Dr. Ling Qi, CARD9 knockout mice and littermate WT mice were a gift from Dr. Stu Levitz, TLR2/4/9 knockout mice and littermate WT mice were a gift from Dr. Tod Merkel, and were validated by RNA-sequencing and functional assays,[82] and TRAF6$^{fl/fl}$ mice were a gift from Dr. Scott Soleimanpour. To generate IRE1$^{\Delta R}$ and control IRE1 WT macrophages, iBMDM from IRE1$^{fl/fl\ exon20\text{-}21}$ mice with and without inducible Cre expression were treated with 4-hydroxy tamoxifen for 24 h, followed by clonal expansion of cell lines. IRE1$^{\Delta R}$ macrophages were confirmed by immunoblotting and *Xbp1* splicing assays. To generate TRAF6 KO cell lines, first lentiviral particles encoding GFP or CRE-GFP were generated by harvesting supernatant 72 h post-transfection of 293T cells with pLEX-FLAG-GFP, or pLEX-FLAG-Cre-GFP, and the packaging plasmids psPAX2 and pMD2.G (provided by Dr. Stacy Horner). These supernatants were then used to transduce TRAF6$^{fl/fl}$ iBMDM for 24 h. Following transduction, cells were selected in 3 μg/mL puromycin (Sigma) for 48 h and single cell colonies were isolated. TRAF6 deletion in CRE-GFP cell lines was verified by immunoblotting in CRE-GFP expressing TRAF6$^{fl/fl}$

iBMDM clonal cell lines (KO-1 and KO-2). GFP-expressing TRAF6$^{fl/fl}$ iBMDM clonal cell lines were used as a control (WT-1 and WT-2).

***Candida albicans* infection, methicillin-resistant *Staphylococcus aureus* (MRSA) infection, and LPS treatment:** *C. albicans* cells were cultured at 30°C in YPD liquid media (1% yeast extract, 2% peptone, 2% dextrose) with constant agitation. All strains were maintained as frozen stocks of 25% glycerol at −80°C. For infection of iBMDM, macrophages were seeded in experimental plates overnight at approximately 80% confluence. Experimental media (RPMI (Gibco), supplemented with 3% FBS) was inoculated with log-phase *C. albicans* yeast cells counted for a calculated MOI of 1. MRSA infection: *Staphylococcus aureus* strain (MRSA), An isogenic strain of MRSA USA300 LAC, a community associated methicillin-resistant harboring p*SarA*-mCherry plasmid (MRSA-mCherry)[73] was cultured at 37°C in tryptic soy broth overnight with constant agitation. Experimental media was inoculated with MRSA at an MOI of 10, as determined by OD600. LPS from *E. coli* O111:B4 (Sigma-Aldrich L2630) was diluted to 100 ng/mL in experimental media for all experiments.

Mice: All mice used for cell line generation or *in vivo* experimentation are C57BL/6J genetic background. For *in vivo C. albicans* experiments, 8–12 week old male and female C57BL/6J mice lacking IRE1α activity in macrophages and neutrophils (IRE1$^{fl/fl}$ LysM^{Cre}) and littermate controls (IRE1$^{fl/fl}$) were used. Mice were housed in the University of Michigan pathogen-free animal facility, and all protocols were approved by and in compliance with the guidelines established by the IACUC (PRO00010463 and PRO00011163) at the University of Michigan.

METHOD DETAILS

Plasmids: pLEX-FLAG-Cre-GFP was generated by cloning PCR-amplified N-terminal FLAG tagged Cre-GFP (from pCAG-Cre-GFP; Addgene #13776) (Forward primer: TAAAGCGGCCGCTATGGCCAATTTACTGACCG; Reverse primer: CTCTAGACTCGAGTTAACTTACTT GTACAGCTCGTCCA) coding sequence into the pLEX expression vector using NotI and XhoI restriction sites. pLEX-FLAG-GFP vector was a gift from Dr. Stacy Horner. All plasmids were verified by whole plasmid sequencing (Plasmidsaurus).

RT-qPCR: Total cellular RNA was extracted from all samples using TRIzol (Thermo Fisher Scientific), according to manufacturer's protocol. RNA was then reverse transcribed using the iScript cDNA synthesis kit (Bio-Rad) as per the manufacturer's instructions. The resulting cDNA was diluted 1:5 in nuclease-free H_2O. RT-qPCR was performed in triplicate using the PowerUP SYBR Green PCR master mix (Thermo Fisher Scientific) and the Bio-Rad CFX Opus 384 Real-Time RT-PCR systems. *Xbp1-S* transcript was amplified using primers Forward: GCTGAGTCCGCAGCAGGT and Reverse: CAGGGTCCAACTTGTCCAGAAT. *Gapdh* transcript was amplified using primers Forward: CATCACTGCCACCCAGAAGACTG and Reverse: ATGCCAGTGAGCTTCCCGTTCAG. *Ddit3* transcript was amplified using primers Forward: GGAGGTCCTGTCCTCAGATGAA and

Reverse: GCTCCTCTGTCAGCCAAGCTAG. *Grp78* transcript was amplified using primers Forward: GTGTTCAAGAACGGCCGCGTG and Reverse: GTTTGCCCACCTCCAATATCAAC. *Grp94* transcript was amplified using primers Forward: GTTTCCCGTGAGACTCTTCAGC and Reverse: ATTCGTGCCGA ACTCCTTCCAG. *Xbp1-T* transcript was amplified using primers Forward: TGAAAAACAGAGTAGCAGCGCAGA and Reverse: CCCAAGCGTGTTCTTAACTC.

Semi-quantitative *Xbp1* splicing gel analysis: Total cellular RNA was extracted using TRIzol (Thermo Fisher Scientific), according to the manufacturer's protocol. RNA was then reverse transcribed using the iScript cDNA synthesis kit (Bio-Rad) as per the manufacturer's instructions. The resulting cDNA was diluted 1:5 in nuclease-free H2O. *Xbp1* transcript was amplified by PCR using primers XF and XR, followed by PCR cleanup using the Qiagen PCR Cleanup Kit. The amplified *Xbp1* product was then digested using PstI, which recognizes a cleavage site within the 26 base pair intron that is removed by IRE1α activity.[83] Following digestion, *Xbp1* bands were resolved on a 2% agarose gel and visualized by ethidium bromide staining and imaging on a BioRad gel dock.

Immunoblotting: Cells were lysed in a modified radioimmunoprecipitation assay (RIPA) buffer (10 mM Tris [pH 7.5], 150 mM NaCl, 0.5% sodium deoxycholate, and 1% Triton X-100) supplemented with protease and phosphatase inhibitor cocktail (Millipore-Sigma) and clarified lysates were harvested by centrifugation. Quantified protein (between 5 and 15 mg) was added to a 4X SDS protein sample buffer (40% glycerol, 240 mM Tris-HCl [pH 6.8], 8% SDS, 0.04% bromophenol blue, 5% beta-mercaptoethanol), resolved by SDS/PAGE, and transferred to nitrocellulose membranes in a 25 mM Tris-192 mM glycine-0.01% SDS buffer. Membranes were stained with Revert 700 total protein stain (LI-COR Biosciences), then blocked in 3% bovine serum albumin. Membranes were incubated with primary antibodies for 2 h at room temperature or overnight at 4C. After washing with PBS-T buffer (1 3 PBS, 0.05% Tween 20), membranes were incubated with species-specific IRDye-conjugated antibodies (Licor, 1:5000) for 1 h at room temperature, followed by imaging on an Odyssey imaging system (LI-COR Biosciences). The following antibodies were used for immunoblotting: rabbit anti-IRE1α (Cell Signaling 3294, 1:1000); rabbit anti-XBP1 (Abcam AB-37152, 1:1000); rabbit anti-CARD9 (Cell Signaling 12283); mouse anti-ACTIN (ThermoFisher ACTN05 (C4); MA5-11869, 1:5000); rabbit anti-TRAF6 (Abcam ab40675, 1:1000); rabbit anti-CARD9 (Cell Signaling 12283, 1:1000); rabbit anti-K48-linkage specific Polyubiquitin antibody (Cell Signaling 4289, 1:1000); rabbit anti-ATF6 (Cell Signaling 65880S, 1:1000); rabbit anti-phospho-eIF2α Ser51 (Cell Signaling 9721, 1:1000); mouse anti-eIF2α (Cell Signaling 2103); rabbit anti-ATF4 (Cell Signaling 11815, 1:1000).

Thioflavin T assay: iBMDM ($2*10^5$ cells/well) were seeded in a 24-well plate overnight and then infected with *C. albicans*, or treated with LPS or thapsigargin for indicated timepoints. Thioflavin T (Cayman Chemical, 5 μM) was added 2 h prior to endpoint. Cells were scraped into ice-cold PBS and thioflavin T intensity was measured on a BD LSRFortessa X-20 flow cytometer.

RNA-sequencing: iBMDM were seeded in 6-well plates overnight (10^6 cells/well) then infected with *C. albicans* (MOI 1) or mock treated (4 h), then harvested in TRIzol reagent (Thermo Fisher) and RNA extraction was performed according to manufacturer protocol. Samples were then treated with Turbo DNase I (Thermo Fisher) according to manufacturer protocol and incubated at 37°C for 30 min, followed by phenol/chloroform extraction and ethanol precipitation overnight. RNA concentrations were then normalized. PolyA enrichment was performed and sequencing libraries were prepared and sequenced on an Illumina NovaSeq 6000 with 150 bp paired-end reads by Novogene.

ELISA: iBMDM ($3*10^4$ cells/well) were seeded in 96-well plates overnight, then primed with LPS (100 ng/mL) for 3 h prior to *C. albicans* infection (MOI 1). Supernatants were collected at 5 hpi and submitted to the University of Michigan Cancer Center Immunology Core for quantification of secreted IL-1β, TNF, and IL-6.

Phagocytosis of *C. albicans* assay: iBMDM ($3*10^4$ cells/well) were seeded in a 96-well plastic-bottom imaging plate (PerkinElmer) overnight and then infected with *C. albicans* (MOI 1) for 30 min. Wells were then fixed in 4% parafolmaldehyde (Electron Microscopy Sciences) for 15 min, washed with PBS (ThermoFisher), and blocked with PBS containing 3% bovine serum albumin (ThermoFisher) and 5% normal goat serum (Invitrogen) for 30 min. FITC-conjugated anti-*Candida* antibody (LSBio LS-C103355, 1:2000) was diluted in blocking buffer and added for 1 h with agitation to label extracellular *C. albicans*, followed by 3 5 min washes with PBS. Wells were then permeabilized in 0.1% Triton X-100 (Sigma-Aldrich) for 15 min, followed by 3 washes in PBS. Calcofluor white (Sigma-Aldrich, 1:100) was diluted in blocking buffer and added to wells for 30 min with agitation, followed by 3 5 min PBS washes, and images were captured on a BioTek Lionheart FX automated microscope.

Phagolysosomal fusion assay: iBMDM ($3*10^4$ cells/well) were seeded in a 96-well plastic-bottom imaging plate (PerkinElmer) overnight and then infected with *C. albicans* SC5314 cells expressing near-infrared fluorescent protein (iRFP) driven by the *pENO1* promoter[74] (MOI 1) at indicated timepoints. Wells were then fixed in 4% paraformaldehyde (Electron Microscopy Sciences) for 15 min, washed with PBS (ThermoFisher), and permeabilized in 0.1% Triton X-100 (Sigma-Aldrich) for 15 min, followed by 3 washes in PBS. Wells were blocked with PBS containing 0.01% Triton X-100, 3% bovine serum albumin (ThermoFisher) and 5% normal goat serum (Invitrogen) for 30 min. Primary antibodies rat anti-LAMP1 (DSHB 1D4B, 1:50) and rabbit anti-LC3 (MBL pM036, 1:400) were diluted in block buffer and added to wells for 1 h, followed by 3 5 min washes with PBS. Alexafluor-conjugated secondary antibodies goat anti-rat 594 and goat anti-rabbit 488 were diluted 1:500 in blocking buffer with DAPI (1:1000) and added to wells for 1 h, followed by 3 5 min PBS washes, and images were captured on a Yokogawa CellVoyager CQ1 automated confocal microscope.

Calcium flux assay and analysis: iBMDM ($3*10^4$ cells/well) were seeded in a 96-well plastic-bottom imaging plate (PerkinElmer) overnight and then loaded with Fluo-4 (1:1000; Fluo-4 Calcium Imaging Kit; Invitrogen) and CellTracker Red (1:2000; Invitrogen)

according to manufacturer protocol for 20 min at 37°C, then 20 min at room temperature. Staining media was then removed, followed by a wash with room temperature media. Cells were infected with *C. albicans* SC5314 cells expressing near-infrared fluorescent protein (iRFP) driven by the *pENO1* promoter[74] (MOI 2), MRSA-mCherry (MOI 1), or Fluorospheres (ThermoFisher F8801) at a 1:10,000 dilution, immediately followed by live imaging captured on a Yokogawa CellVoyager CQ1 automated confocal microscope with incubation at 37°C with 5% CO_2. Images were captured every 90 s for 1 h.

Macrophage fungicidal activity assay (live imaging): iBMDM ($3*10^4$ cells/well) were seeded in a 96-well plastic-bottom imaging plate (PerkinElmer) overnight. Approximately 10^7 *C albicans* SC5314 cells expressing iRFP from an overnight culture were stained with calcofluor white (CFW; 100 μg/mL) for 10 min in the dark. Cells were then washed twice with PBS prior to macrophage infection at MOI = 1. Images of infected cultures were captured every 20 min on a BioTek Lionheart FX automated microscope with incubation at 37C and 5% CO2. Fungal killing was quantified at 7 h post-infection by calculating killed *C. albicans* ($iRFP^-$ CFW^+) over total *C. albicans* ($iRFP^{-/+}$ CFW^+), with at least 200 *C albicans* cells counted per condition.

Macrophage fungicidal activity assay (endpoint): iBMDM ($3*10^4$ cells/well) were seeded in a 96-well plastic-bottom imaging plate (PerkinElmer) overnight. Approximately 10^7 *C albicans* SC5314 cells expressing iRFP from an overnight culture were stained with calcofluor white (CFW; 100 μg/mL) for 10 min in the dark. Cells were then washed twice with PBS prior to macrophage infection at MOI = 1. Images of infected cultures were captured every 20 min on a BioTek Lionheart FX automated microscope with incubation at 37°C and 5% CO2.

LysoSensor: iBMDM ($2*10^5$ cells/well) were seeded in a 24-well plate overnight and then infected with *C. albicans* for 2 h prior to addition of LysoSensor Yellow/Blue DND-160 (Thermo Fisher, 500 nM) for 2 min in experimental media. Wells were then washed 3 times in ice-cold PBS and scraped for plate reader analysis. Suspended cells were added to a black-bottom 96-well plate and absorbance and emission were measured at 329 nm Abs, 440 nm Em and 384 nm Abs, 540 nm Em to measure fluorescence intensity in high and low pH environments, respectively. The intensity of the low pH measurement was divided by the intensity of the high pH measurement, and these results were normalized to IRE1 WT Mock to determine the relative acidity of each condition.

LysoTracker: iBMDM ($3*10^4$ cells/well) were seeded in a 96-well plastic-bottom imaging plate (PerkinElmer) overnight, then treated with NH4Cl (20 mM) or DMSO as a control for 2 h. Media was then replaced with treatment media containing LysoTracker (500 nM) and Hoechst (1 μg/mL) for 10 min at 37°C for 10 min. LysoTracker was then washed out twice with warm media, and cells were imaged on a Yokogawa CellVoyager CQ1 automated confocal microscope.

Sulforhodamine B assay and *C. albicans* hyphal length measurement: iBMDM ($3*10^4$ cells/well) were seeded in a 96-well plastic-bottom imaging plate (PerkinElmer) overnight, then sulforhodamine B (SRB) (Sigma-Aldrich, 150 μg/mL) was added to wells

for 1 h. SRB was then washed out and wells were with *C. albicans* expressing iRFP (MOI 1) and live imaging was performed on a Yokogawa CellVoyager CQ1 automated confocal microscope every 30 min for 5 h.

Proximity ligation assay: iBMDM ($1*10^4$ cells/well) were seeded in a 384-well plastic-bottom imaging plate (PerkinElmer) overnight, then mock treated or infected with *C. albicans* (MOI 1) for 1 h. Wells were then fixed in 4% paraformaldehyde (Electron Microscopy Sciences) for 15 min, washed with PBS (ThermoFisher), and permeabilized in 0.1% Triton X-100 (Sigma-Aldrich) for 15 min, followed by 3 washes in PBS. Proximity ligation assay was performed using the Duolink *In Situ* PLA kit (Sigma-Aldrich) according to manufacturer instructions. Wells were blocked using PLA Blocking Solution for 1 h at 37°C, followed by incubation with primary antibodies diluted in Duolink Antibody Dilutent: mouse anti-EEA1 (ThermoFisher MA5-31575; 1:200) and rabbit anti-KDEL (Abcam ab176333; 1:200) for 2 h at room temperature, followed by 3 5 min washes with Wash Buffer A. PLA probes (anti-mouse minus and anti-rabbit plus) were diluted 1:5 in Duolink Antibody Diluent and added to wells for 1 h at 37°C, followed by 3 5 min washes with Wash Buffer A. Duolink Ligation buffer was diluted 1:5 in Ultrapure water with Ligase at 1:40 dilution and added to wells for 30 min at 37°C, followed by 3 5 min washes with Wash Buffer A. Duolink Amplification buffer was diluted 1:5 in Ultrapure water with Polymerase at 1:80 dilution and added to wells for 100 min at 37°C, followed by 3 10 min washes in Wash Buffer B. DAPI (1:1000) was then added to wells in Wash Buffer B for 10 min, followed by a 1 min wash in 0.01X Wash Buffer B. Wells were resuspended in PBS and imaged on a Yokogawa CellVoyager CQ1 automated confocal microscope or Nikon X1 spinning disk confocal microscope.

***In vivo* systemic *C. albicans* challenge experiments:** Overnight cultures of *C. albicans* expressing iRFP were sub-cultured at a starting OD600 of 0.1 and grown for 4 h to mid-log phase growth, then pelleted by centrifugation and resuspended in PBS for delivery to the bloodstream of mice. 8–12 week old male and female mice lacking IRE1α activity in macrophages and neutrophils ($IRE1^{fl/fl}$ $LysM^{Cre}$) and littermate controls ($IRE1^{fl/fl}$) were systemically infected with iRFP-expressing *C. albicans* (10^6 CFU) by retro-orbital injection. At 24 h post-infection, mice were euthanized and serum was collected by cardiac puncture, followed by isolation of serum using centrifugation of serum collection tubes. Serum samples were submitted to the University of Michigan Cancer Center Immunology Core for quantification of secreted IL-1β, IL-1Ra, TNF, and IL-6 by ELISA. Kidneys were isolated and dissociated by mechanical separation through a 70 μm cell strainer, followed by red blood cell lysis (eBioscience 10X RBC Lysis Buffer). To quantify *C. albicans* viability in kidney samples, $2*10^6$ cells per sample were subjected to immunofluorescence staining. Total *C. albicans* was stained using a FITC-conjugated anti-*Candida* antibody (1:1000; Meridian Bioscience), and myeloid cells were stained with Brilliant Violet 421-conjugated Rat anti-CD11b antibody (1:100; Biolegend 414-0112-82) for 1 h in the dark with gentle agitation. After immunostaining, samples were plated in 96-well plastic-bottom imaging plates (PerkinElmer) coated with poly-D-Lysine (Gibco) and imaging was performed on a Yokogawa CellVoyager CQ1 automated confocal microscope. Mice were housed in the University of Michigan pathogen-free animal facility, and all protocols were approved

by and in compliance with the guidelines established by the IACUC (PRO00010463 and PRO00011163) at the University of Michigan.

QUANTIFICATION AND STATISTICAL ANALYSIS

Quantification of immunoblots: Following imaging using the LI-COR Odyssey imager, immunoblots were quantified using ImageStudio Lite software, and raw values were normalized to total protein (Revert 700 total protein stain) or ACTIN for each condition.

RNA-seq analysis: RNA-seq analysis was performed in Galaxy (usegalaxy.org). Reads were evaluated using FastQC and trimmed using cutadapt,[78] followed by quantification of transcripts from the GRCm38 mouse genome using Kallisto.[79] Differential gene expression between IRE1$^{\Delta R}$ and IRE1 WT macrophages following *C. albicans* infection (Table S1.1) was compared using DESeq2.[80] Gene ontology analysis was performed on significantly upregulated or downregulated genes in each dataset using g:Profiler.[84]

Quantification of phagocytosis of C. albicans: A CellProfiler[75] pipeline (Data S1) was developed to segment extracellular (FITC+) and total (FITC+ CFW+) *C. albicans*, and the percent phagocytosed by macrophages was calculated as 100 * (1 − (FITC+/FITC+ CFW+)).

Quantification of phagolysosomal fusion: A CellProfiler pipeline (Data S1) was developed to segment *C. albicans* and measure the mean intensity of LAMP1 enriched at the *C. albicans* network.

Quantification of calcium flux: Analysis of initial Fluo-4 intensity was performed on time 0 images using a CellProfiler pipeline to identify cells and measure the mean fluorescence intensity of Fluo-4. For analysis of cellular calcium flux, the Python package spacr (https://github.com/EinarOlafsson/spacr) was used to segment and track cells over time and quantify single cell calcium oscillations. Cells were delineated with the Cellpose cyto model[77] from CellTracker Red staining. Centroids of identified cell objects were tracked using the Trackpy particle-tracking algorithm.[85] Fluo-4 mean intensity values were normalized between 0 and 1 and corrected for photobleaching across the time series using an exponential decay model to enable the detection of calcium spikes above a threshold of 0.25 with the find_peaks function from scipy.[86] Peaks were then enumerated and characterized by collecting peak frequency and amplitude for each condition.

Analysis of phagosomal calcium influx was performed at 20 min post-infection using NIH Fiji/ImageJ.[76] The line tool was used to calculate the mean fluorescence intensity of Fluo4 rings within *C. albicans*-containing phagosomes, which were measured relative to the mean fluorescence intensity of the whole parental macrophage. Calcium-high phagosomes were defined as phagosomes with Fluo-4 intensity >1.25-fold higher than the mean fluorescence intensity of the parent macrophage. Additionally, CellProfiler pipelines were developed to measure relative phagosomal Fluo4 intensity, normalized to cytoplasmic Fluo4 intensity, for *C. albicans* infection and MRSA infection (Data S1), as shown in Figures S9 and S10.

Quantification of macrophage fungicidal activity (endpoint): Fungal killing was quantified at 7 h post-infection by calculating killed *C. albicans* (iRFP^{-} FITC^{+}) over total *C. albicans* (iRFP$^{-/+}$ FITC^{+}), with at least 200 *C albicans* cells counted per condition. A CellProfiler pipeline (Data S1) was developed to segment *C. albicans*. Total *C. albicans* were identified using FITC signal, and viability was measured using iRFP intensity.

Quantification of LysoTracker signal: Nuclei and lysosomes were segmented using a CellProfiler pipeline (Data S1) and the integrated intensity of LysoTracker was measured on a single-cell basis and plotted relative to WT Mock.

Quantification of sulforhodamine B assay and C. albicans hyphal growth: A CellProfiler pipeline (Data S1) was developed to segment *C. albicans* and measure the total area covered by hyphae, and the mean intensity of SRB enriched at the *C. albicans* network was measured at each timepoint.

Quantification of proximity ligation assay puncta: A CellProfiler pipeline (Data S1) was developed to segment PLA puncta and *C. albicans* and measure the average number of PLA puncta per cell (PLA puncta/nuclei).

Quantification of C. albicans killing *in vivo*: A CellProfiler pipeline (Data S1) was developed to segment *C. albicans* and host myeloid cells. Total *C. albicans* were identified from kidney tissue and myeloid cells using FITC signal, and viability was measured using iRFP intensity.

Statistical analysis: Statistical analyses were performed using GraphPad Prism software. Details for individual figures are as follows.

Figure 1. *$p < 0.05$, **$p < 0.01$, ***$p < 0.005$ by two-way ANOVA of log-transformed data with Sidak's multiple comparisons test. ns, not significant.

Figure 2. *$p < 0.05$, **$p < 0.01$, ***$p < 0.005$ by two-way ANOVA with Sidak's multiple comparisons test of log-transformed data (A, B), one-way ANOVA with Tukey's multiple comparisons test (D-F), or one-way ANOVA with Dunnett's multiple comparisons test (G-H). Graphs show the mean ± SEM of biological replicates.

Figure 3. **$p < 0.05$, **$p < 0.01$ by unpaired Student's t test (B, E-F) or by two-way ANOVA with Dunnett's multiple comparisons test (C).

Figure 4. *$p < 0.05$, *$p < 0.01$ by two-way ANOVA with Tukey's multiple comparisons test (B), one-way ANOVA (C) or unpaired Student's t test (E).

Figure 5. *$p < 0.05$, **$p < 0.01$, ***$p < 0.001$, ns not significant by unpaired Student's t-test (B-C, F) or one-way ANOVA with Tukey's multiple comparisons test (D).

Supplementary Material

Refer to Web version on PubMed Central for supplementary material.

ACKNOWLEDGMENTS

We thank the following colleagues who provided cell lines and reagents: Dr. Stacy Horner, Dr. Ling Qi, Dr. Stu Levitz, Dr. Tod Merkel, and Dr. Scott Soleimanpour. We also thank Dr. Basel Abuaita for immortalization of IRE1$^{fl/fl\ exon20\text{-}21}$ and TLR2/4/9 KO macrophages and matched controls. We thank the members of the O'Meara and O'Riordan labs for discussion. This work was supported by National Institutes of Health grant nos. K22 AI137299 (T.R.O.), R01 AI157384 (M.X.D.O.), T32AR007197 (M.J.M.), and T32AI007528 (M.J.M.). Other funding was provided by the University of Michigan Pioneer Fellows Program (M.J.M.).

REFERENCES

1. Muralidharan S, and Mandrekar P. (2013). Cellular stress response and innate immune signaling: integrating pathways in host defense and inflammation. J. Leukoc. Biol 94, 1167–1184. [PubMed: 23990626]
2. Chovatiya R, and Medzhitov R. (2014). Stress, inflammation, and defense of homeostasis. Mol. Cell 54, 281–288. [PubMed: 24766892]
3. Grootjans J, Kaser A, Kaufman RJ, and Blumberg RS (2016). The unfolded protein response in immunity and inflammation. Nat. Rev. Immunol 16, 469–484. [PubMed: 27346803]
4. Choi J-A, and Song C-H (2019). Insights Into the Role of Endoplasmic Reticulum Stress in Infectious Diseases. Front. Immunol 10, 3147. [PubMed: 32082307]
5. Read A, and Schröder M. (2021). The Unfolded Protein Response: An Overview. Biology 10, 384. [PubMed: 33946669]
6. Yoshida H, Matsui T, Yamamoto A, Okada T, and Mori K. (2001). XBP1 mRNA is induced by ATF6 and spliced by IRE1 in response to ER stress to produce a highly active transcription factor. Cell 107, 881–891. [PubMed: 11779464]
7. Cox JS, and Walter P. (1996). A novel mechanism for regulating activity of a transcription factor that controls the unfolded protein response. Cell 87, 391–404. [PubMed: 8898193]
8. Kaufman RJ (1999). Stress signaling from the lumen of the endoplasmic reticulum: coordination of gene transcriptional and translational controls. Genes Dev. 13, 1211–1233. [PubMed: 10346810]
9. Belyy V, Zuazo-Gaztelu I, Alamban A, Ashkenazi A, and Walter P. (2022). Endoplasmic reticulum stress activates human IRE1α through reversible assembly of inactive dimers into small oligomers. Elife 11, e74342. [PubMed: 35730415]
10. Park S-M, Kang T-I, and So J-S (2021). Roles of XBP1s in Transcriptional Regulation of Target Genes. Biomedicines 9, 791. [PubMed: 34356855]
11. Urano F, Wang X, Bertolotti A, Zhang Y, Chung P, Harding HP, and Ron D. (2000). Coupling of stress in the ER to activation of JNK protein kinases by transmembrane protein kinase IRE1. Science 287, 664–666. [PubMed: 10650002]
12. Carreras-Sureda A, Zhang X, Laubry L, Brunetti J, Koenig S, Wang X, Castelbou C, Hetz C, Liu Y, Frieden M, and Demaurex N. (2023). The ER stress sensor IRE1 interacts with STIM1 to promote store-operated calcium entry, T cell activation, and muscular differentiation. Cell Rep. 42, 113540. [PubMed: 38060449]
13. Carreras-Sureda A, Jaña F, Urra H, Durand S, Mortenson DE, Sagredo A, Bustos G, Hazari Y, Ramos-Fernández E, Sassano ML, et al. (2019). Non-canonical function of IRE1α determines mitochondria-associated endoplasmic reticulum composition to control calcium transfer and bioenergetics. Nat. Cell Biol 21, 755–767. [PubMed: 31110288]
14. Iovino M, Colonval M, Wilkin C, L'homme L, Lassence C, Campas M, Peulen O, de Tullio P, Piette J, and Legrand-Poels S. (2023). Novel XBP1s-independent function of IRE1 RNase in HIF-1α-mediated glycolysis upregulation in human macrophages upon stimulation with LPS or saturated fatty acid. Front. Immunol 14, 1204126. [PubMed: 37711626]
15. Martinon F, Chen X, Lee A-H, and Glimcher LH (2010). TLR activation of the transcription factor XBP1 regulates innate immune responses in macrophages. Nat. Immunol 11, 411–418. [PubMed: 20351694]
16. Qiu Q, Zheng Z, Chang L, Zhao YS, Tan C, Dandekar A, Zhang Z, Lin Z, Gui M, Li X, et al. (2013). Toll-like receptor-mediated IRE1α activation as a therapeutic target for inflammatory arthritis. EMBO J. 32, 2477–2490. [PubMed: 23942232]

17. Nguyen LC, Renner DM, Silva D, Yang D, Parenti N, Medina KM, Nicolaescu V, Gula H, Drayman N, Valdespino A, et al. (2022). SARS-CoV-2 diverges from other betacoronaviruses in only partially activating the IRE1α/XBP1 ER stress pathway in human lung-derived cells. Preprint at bioRxiv. 10.1101/2021.12.30.474519.

18. English BC, Savage HP, Mahan SP, Diaz-Ochoa VE, Young BM, Abuaita BH, Sule G, Knight JS, O'Riordan MX, Bäumler AJ, and Tsolis RM (2023). The IRE1α-XBP1 Signaling Axis Promotes Glycolytic Reprogramming in Response to Inflammatory Stimuli. mBio 14, e0306822. [PubMed: 36475773]

19. Yu C-Y, Hsu Y-W, Liao C-L, and Lin Y-L (2006). Flavivirus infection activates the XBP1 pathway of the unfolded protein response to cope with endoplasmic reticulum stress. J. Virol 80, 11868–11880. [PubMed: 16987981]

20. Abuaita BH, Burkholder KM, Boles BR, and O'Riordan MX (2015). The Endoplasmic Reticulum Stress Sensor Inositol-Requiring Enzyme 1α Augments Bacterial Killing through Sustained Oxidant Production. mBio 6, e00705. [PubMed: 26173697]

21. Abuaita BH, Schultz TL, and O'Riordan MX (2018). Mitochondria-Derived Vesicles Deliver Antimicrobial Reactive Oxygen Species to Control Phagosome-Localized Staphylococcus aureus. Cell Host Microbe 24, 625–636.e5. [PubMed: 30449314]

22. Bronner DN, Abuaita BH, Chen X, Fitzgerald KA, Nuñez G, He Y, Yin XM, and O'Riordan MXD (2015). Endoplasmic Reticulum Stress Activates the Inflammasome via NLRP3- and Caspase-2-Driven Mitochondrial Damage. Immunity 43, 451–462. [PubMed: 26341399]

23. Anderson FM, Visser ND, Amses KR, Hodgins-Davis A, Weber AM, Metzner KM, McFadden MJ, Mills RE, O'Meara MJ, James TY, and O'Meara TR (2023). Candida albicans selection for human commensalism results in substantial within-host diversity without decreasing fitness for invasive disease. PLoS Biol. 21, e3001822. [PubMed: 37205709]

24. Awasthi D, Chopra S, Cho BA, Emmanuelli A, Sandoval TA, Hwang SM, Chae CS, Salvagno C, Tan C, Vasquez-Urbina L, et al. (2023). Inflammatory ER stress responses dictate the immunopatho-genic progression of systemic candidiasis. J. Clin. Investig 133, e167359. 10.1172/JCI167359. [PubMed: 37432737]

25. Lionakis MS, Swamydas M, Fischer BG, Plantinga TS, Johnson MD, Jaeger M, Green NM, Masedunskas A, Weigert R, Mikelis C, et al. (2013). CX3CR1-dependent renal macrophage survival promotes Candida control and host survival. J. Clin. Investig 123, 5035–5051. [PubMed: 24177428]

26. van de Veerdonk FL, Gresnigt MS, Oosting M, van der Meer JWM, Joosten LAB, Netea MG, and Dinarello CA (2014). Protective host defense against disseminated candidiasis is impaired in mice expressing human interleukin-37. Front. Microbiol 5, 762. [PubMed: 25620965]

27. Netea MG, Joosten LAB, van der Meer JWM, Kullberg B-J, and van de Veerdonk FL (2015). Immune defence against Candida fungal infections. Nat. Rev. Immunol 15, 630–642. [PubMed: 26388329]

28. Hise AG, Tomalka J, Ganesan S, Patel K, Hall BA, Brown GD, and Fitzgerald KA (2009). An essential role for the NLRP3 inflammasome in host defense against the human fungal pathogen Candida albicans. Cell Host Microbe 5, 487–497. [PubMed: 19454352]

29. Joly S, Ma N, Sadler JJ, Soll DR, Cassel SL, and Sutterwala FS (2009). Cutting edge: Candida albicans hyphae formation triggers activation of the Nlrp3 inflammasome. J. Immunol 183, 3578–3581. [PubMed: 19684085]

30. Gross O, Poeck H, Bscheider M, Dostert C, Hannesschläger N, Endres S, Hartmann G, Tardivel A, Schweighoffer E, Tybulewicz V, et al. (2009). Syk kinase signalling couples to the Nlrp3 inflammasome for anti-fungal host defence. Nature 459, 433–436. [PubMed: 19339971]

31. Wellington M, Koselny K, and Krysan DJ (2012). Candida albicans morphogenesis is not required for macrophage interleukin 1β production. mBio 4, e00433–12. [PubMed: 23269828]

32. Wellington M, Koselny K, Sutterwala FS, and Krysan DJ (2014). Candida albicans triggers NLRP3-mediated pyroptosis in macrophages. Eukaryot. Cell 13, 329–340. [PubMed: 24376002]

33. O'Meara TR, Veri AO, Ketela T, Jiang B, Roemer T, and Cowen LE (2015). Global analysis of fungal morphology exposes mechanisms of host cell escape. Nat. Commun 6, 6741. [PubMed: 25824284]

34. Newman SL, Bhugra B, Holly A, and Morris RE (2005). Enhanced killing of Candida albicans by human macrophages adherent to type 1 collagen matrices via induction of phagolysosomal fusion. Infect. Immun 73, 770–777. [PubMed: 15664915]
35. Westman J, Walpole GFW, Kasper L, Xue BY, Elshafee O, Hube B, and Grinstein S. (2020). Lysosome Fusion Maintains Phagosome Integrity during Fungal Infection. Cell Host Microbe 28, 798–812.e6. [PubMed: 33022213]
36. Vesely EM, Williams RB, Konopka JB, and Lorenz MC (2017). N-Acetylglucosamine Metabolism Promotes Survival of Candida albicans in the Phagosome. mSphere 2, e00357–17.
37. Seegren PV, Downs TK, Stremska ME, Harper LR, Cao R, Olson RJ, Upchurch CM, Doyle CA, Kennedy J, Stipes EL, et al. (2020). Mitochondrial Ca2+ Signaling Is an Electrometabolic Switch to Fuel Phagosome Killing. Cell Rep. 33, 108411. [PubMed: 33238121]
38. Iwawaki T, Akai R, Yamanaka S, and Kohno K. (2009). Function of IRE1 alpha in the placenta is essential for placental development and embryonic viability. Proc. Natl. Acad. Sci. USA 106, 16657–16662. [PubMed: 19805353]
39. Glazier VE, Kramara J, Ollinger T, Solis NV, Zarnowski R, Wakade RS, Kim MJ, Weigel GJ, Liang SH, Bennett RJ, et al. (2023). The Candida albicans reference strain SC5314 contains a rare, dominant allele of the transcription factor Rob1 that modulates filamentation, biofilm formation, and oral commensalism. mBio 14, e0152123. [PubMed: 37737633]
40. Netea MG, Brown GD, Kullberg BJ, and Gow NAR (2008). An integrated model of the recognition of Candida albicans by the innate immune system. Nat. Rev. Microbiol 6, 67–78. [PubMed: 18079743]
41. Hardison SE, and Brown GD (2012). C-type lectin receptors orchestrate antifungal immunity. Nat. Immunol 13, 817–822. [PubMed: 22910394]
42. Poltorak A, Smirnova I, He X, Liu MY, Van Huffel C, McNally O, Birdwell D, Alejos E, Silva M, Du X, et al. (1998). Genetic and physical mapping of the Lps locus: identification of the toll-4 receptor as a candidate gene in the critical region. Blood Cells Mol. Dis 24, 340–355. [PubMed: 10087992]
43. Hsu Y-MS, Zhang Y, You Y, Wang D, Li H, Duramad O, Qin XF, Dong C, and Lin X. (2007). The adaptor protein CARD9 is required for innate immune responses to intracellular pathogens. Nat. Immunol 8, 198–205. [PubMed: 17187069]
44. Kawai T, and Akira S. (2010). The role of pattern-recognition receptors in innate immunity: update on Toll-like receptors. Nat. Immunol 11, 373–384. [PubMed: 20404851]
45. Gorjestani S, Darnay BG, and Lin X. (2012). Tumor necrosis factor receptor-associated factor 6 (TRAF6) and TGFβ-activated kinase 1 (TAK1) play essential roles in the C-type lectin receptor signaling in response to Candida albicans infection. J. Biol. Chem 287, 44143–44150. [PubMed: 23148225]
46. Beriault DR, and Werstuck GH (2013). Detection and quantification of endoplasmic reticulum stress in living cells using the fluorescent compound, Thioflavin T. Biochim. Biophys. Acta 1833, 2293–2301. [PubMed: 23747341]
47. Diamond RD, Lyman CA, and Wysong DR (1991). Disparate effects of interferon-gamma and tumor necrosis factor-alpha on early neutrophil respiratory burst and fungicidal responses to Candida albicans hyphae in vitro. J. Clin. Investig 87, 711–720. [PubMed: 1846880]
48. Volkmann K, Lucas JL, Vuga D, Wang X, Brumm D, Stiles C, Kriebel D, Der-Sarkissian A, Krishnan K, Schweitzer C, et al. (2011). Potent and selective inhibitors of the inositol-requiring enzyme 1 endoribonuclease. J. Biol. Chem 286, 12743–12755. [PubMed: 21303903]
49. Harrington PE, Biswas K, Malwitz D, Tasker AS, Mohr C, Andrews KL, Dellamaggiore K, Kendall R, Beckmann H, Jaeckel P, et al. (2015). Unfolded protein response in cancer: IRE1α inhibition by selective kinase ligands does not impair tumor cell viability. ACS Med. Chem. Lett 6, 68–72. [PubMed: 25589933]
50. Feldman HC, Ghosh R, Auyeung VC, Mueller JL, Kim JH, Potter ZE, Vidadala VN, Perera BGK, Olivier A, Backes BJ, et al. (2021). ATP-competitive partial antagonists of the IRE1α RNase segregate outputs of the UPR. Nat. Chem. Biol 17, 1148–1156. [PubMed: 34556859]

51. Borisova E, Newman AG, Couce Iglesias M, Dannenberg R, Schaub T, Qin B, Rusanova A, Brockmann M, Koch J, Daniels M, et al. (2024) Protein translation rate determines neocortical neuron fate. Nat. Commun 15, 4879. [PubMed: 38849354]
52. Medel B, Bernales JI, Lira A, Fernández D, Iwawaki T, Vargas P, and Osorio F. (2023). The unfolded protein response sensor IRE1 regulates activation of in vitro differentiated type 1 conventional DCs with viral stimuli. Int. J. Mol. Sci 24, 10205. [PubMed: 37373353]
53. Ghavami M, and Fairn GD (2022). Endoplasmic reticulum-Phagosome contact sites from the cradle to the grave. Front. Cell Dev. Biol 10, 1074443. [PubMed: 36619860]
54. Vylkova S, and Lorenz MC (2014). Modulation of phagosomal pH by Candida albicans promotes hyphal morphogenesis and requires Stp2p, a regulator of amino acid transport. PLoS Pathog. 10, e1003995. [PubMed: 24626429]
55. Danhof HA, and Lorenz MC (2015). The Candida albicans ATO Gene Family Promotes Neutralization of the Macrophage Phagolysosome. Infect. Immun 83, 4416–4426. [PubMed: 26351284]
56. Boron WF, and De Weer P. (1976). Intracellular pH transients in squid giant axons caused by CO2, NH3, and metabolic inhibitors. J. Gen. Physiol 67, 91–112. [PubMed: 1460]
57. O'Meara TR, Duah K, Guo CX, Maxson ME, Gaudet RG, Koselny K, Wellington M, Powers ME, MacAlpine J, O'Meara MJ, et al. (2018). High-Throughput Screening Identifies Genes Required for Candida albicans Induction of Macrophage Pyroptosis. mBio 9, e01581–18. [PubMed: 30131363]
58. Yang M, Walpole GFW, and Westman J. (2020). Maintaining phagosome integrity during fungal infection: do or die? Microb. Cell 7, 323–325. [PubMed: 33335922]
59. Uwamahoro N, Verma-Gaur J, Shen HH, Qu Y, Lewis R, Lu J, Bambery K, Masters SL, Vince JE, Naderer T, and Traven A. (2014). The pathogen Candida albicans hijacks pyroptosis for escape from macrophages. mBio 5, e00003–e14. [PubMed: 24667705]
60. Mencacci NE, Rubio-Agusti I, Zdebik A, Asmus F, Ludtmann MHR, Ryten M, Plagnol V, Hauser AK, Bandres-Ciga S, Bettencourt C, et al. (2015). A missense mutation in KCTD17 causes autosomal dominant myoclonus-dystonia. Am. J. Hum. Genet 96, 938–947. [PubMed: 25983243]
61. Burk SE, Lytton J, MacLennan DH, and Shull GE (1989). cDNA cloning, functional expression, and mRNA tissue distribution of a third organellar Ca2+ pump. J. Biol. Chem 264, 18561–18568. [PubMed: 2553713]
62. Besprozvannaya M, Dickson E, Li H, Ginburg KS, Bers DM, Auwerx J, and Nunnari J. (2018). GRAM domain proteins specialize functionally distinct ER-PM contact sites in human cells. Elife 7, e31019. [PubMed: 29469807]
63. Wu Y, Huang P, and Dong X-P (2021). Lysosomal Calcium Channels in Autophagy and Cancer. Cancers 13, 1299. [PubMed: 33803964]
64. Westman J, Grinstein S, and Maxson ME (2019). Revisiting the role of calcium in phagosome formation and maturation. J. Leukoc. Biol 106, 837–851. [PubMed: 31091355]
65. Nunes P, Cornut D, Bochet V, Hasler U, Oh-Hora M, Waldburger JM, and Demaurex N. (2012). STIM1 juxtaposes ER to phagosomes, generating Ca^{2+} hotspots that boost phagocytosis. Curr. Biol 22, 1990–1997. [PubMed: 23041196]
66. Rutkowski DT, and Hegde RS (2010). Regulation of basal cellular physiology by the homeostatic unfolded protein response. J. Cell Biol 189, 783–794. [PubMed: 20513765]
67. Dufey E, Bravo-San Pedro JM, Eggers C, González-Quiroz M, Urra H, Sagredo AI, Sepulveda D, Pihán P, Carreras-Sureda A, Hazari Y, et al. (2020). Genotoxic stress triggers the activation of IRE1α-dependent RNA decay to modulate the DNA damage response. Nat. Commun 11, 2401. [PubMed: 32409639]
68. Zhu X, Zhang J, Sun H, Jiang C, Dong Y, Shan Q, Su S, Xie Y, Xu N, Lou X, and Liu S. (2014). Ubiquitination of inositol-requiring enzyme 1 (IRE1) by the E3 ligase CHIP mediates the IRE1/TRAF2/JNK pathway. J. Biol. Chem 289, 30567–30577. [PubMed: 25225294]
69. Raiborg C, Wenzel EM, and Stenmark H. (2015). ER-endosome contact sites: molecular compositions and functions. EMBO J. 34, 1848–1858. [PubMed: 26041457]
70. Kyrmizi I, Ferreira H, Carvalho A, Figueroa JAL, Zarmpas P, Cunha C, Akoumianaki T, Stylianou K, Deepe GS Jr., Samonis G, et al. (2018). Calcium sequestration by fungal melanin inhibits

calcium–calmodulin signalling to prevent LC3-associated phagocytosis. Nat. Microbiol 3, 791–803. [PubMed: 29849062]

71. Sha H, He Y, Yang L, and Qi L. (2011). Stressed out about obesity: IRE1α-XBP1 in metabolic disorders. Trends Endocrinol. Metab 22, 374–381. [PubMed: 21703863]
72. Abram CL, Roberge GL, Hu Y, and Lowell CA (2014). Comparative analysis of the efficiency and specificity of myeloid-Cre deleting strains using ROSA-EYFP reporter mice. J. Immunol. Methods 408, 89–100. [PubMed: 24857755]
73. Boles BR, and Horswill AR (2008). Agr-mediated dispersal of Staphylococcus aureus biofilms. PLoS Pathog. 4, e1000052. [PubMed: 18437240]
74. Ost KS, O'Meara TR, Stephens WZ, Chiaro T, Zhou H, Penman J, Bell R, Catanzaro JR, Song D, Singh S, et al. (2021). Adaptive immunity induces mutualism between commensal eukaryotes. Nature 596, 114–118. [PubMed: 34262174]
75. Stirling DR, Swain-Bowden MJ, Lucas AM, Carpenter AE, Cimini BA, and Goodman A. (2021). CellProfiler 4: improvements in speed, utility and usability. BMC Bioinf. 22, 433.
76. Schindelin J, Arganda-Carreras I, Frise E, Kaynig V, Longair M, Pietzsch T, Preibisch S, Rueden C, Saalfeld S, Schmid B, et al. (2012). Fiji: an open-source platform for biological-image analysis. Nat. Methods 9, 676–682. [PubMed: 22743772]
77. Stringer C, Wang T, Michaelos M, and Pachitariu M. (2021). Cellpose: a generalist algorithm for cellular segmentation. Nat. Methods 18, 100–106. [PubMed: 33318659]
78. Martin M. (2011). Cutadapt removes adapter sequences from high-throughput sequencing reads. EMBnet. j 17, 10.
79. Bray NL, Pimentel H, Melsted P, and Pachter L. (2016). Near-optimal probabilistic RNA-seq quantification. Nat. Biotechnol 34, 525–527. [PubMed: 27043002]
80. Love MI, Huber W, and Anders S. (2014). Moderated estimation of fold change and dispersion for RNA-seq data with DESeq2. Genome Biol. 15, 550. [PubMed: 25516281]
81. Blasi E, Radzioch D, Merletti L, and Varesio L. (1989). Generation of macrophage cell line from fresh bone marrow cells with a myc/raf recombinant retrovirus. Cancer Biochem. Biophys 10, 303–317. [PubMed: 2695237]
82. Reynolds MB, Klein B, McFadden MJ, Judge NK, Navarrete HE, Michmerhuizen BC, Awad D, Schultz TL, Harms PW, Zhang L, et al. (2024). Type I interferon governs immunometabolic checkpoints that coordinate inflammation during Staphylococcal infection. Cell Rep. 43, 114607. [PubMed: 39126652]
83. Hirota M, Kitagaki M, Itagaki H, and Aiba S. (2006). Quantitative measurement of spliced XBP1 mRNA as an indicator of endoplasmic reticulum stress. J. Toxicol. Sci 31, 149–156. [PubMed: 16772704]
84. Reimand J, Kull M, Peterson H, Hansen J, and Vilo J. (2007). Profiler–a web-based toolset for functional profiling of gene lists from large-scale experiments. Nucleic Acids Res. 35, W193–W200. [PubMed: 17478515]
85. Allan DB, Caswell T, Keim NC, van der Wel CM & Verweij RW (2024). soft-matter/trackpy. Zenodo 10.5281/zenodo.10696534.
86. Virtanen P, Gommers R, Oliphant TE, Haberland M, Reddy T, Cournapeau D, Burovski E, Peterson P, Weckesser W, Bright J, et al. (2020). Author Correction: SciPy 1.0: fundamental algorithms for scientific computing in Python. Nat. Methods 17, 352. [PubMed: 32094914]

Highlights

- *C. albicans* infection drives protein-misfolding-independent activation of IRE1α
- IRE1α enhances calcium flux at the *C. albicans*-containing phagosome
- IRE1α promotes phagosome maturation and integrity
- IRE1α augments macrophage fungicidal activity

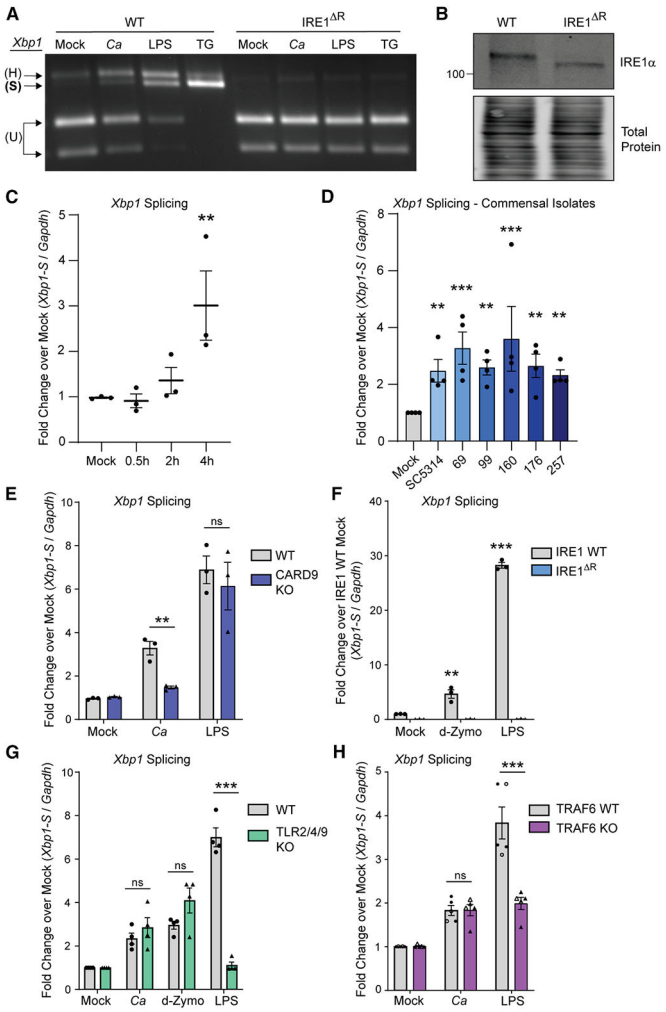

Figure 1. *Candida albicans* infection results in activation of macrophage IRE1α

(A) iBMDM cell lines (WT or IRE1$^{\Delta R}$) were infected with *C. albicans* (*Ca*), treated with LPS, thapsigargin, or mock for 4 h. *Xbp1* mRNA splicing was measured by semi-quantitative RT-PCR amplification of the *Xbp1* transcript, followed by treatment with PstI, which recognizes a cleavage site within the 26-bp intron that is removed by IRE1α, resulting in cleavage of the unspliced isoform, specifically.

(B) Immunoblot analysis of lysates from WT or IRE1$^{\Delta R}$ iBMDM to confirm IRE1α truncation in IRE1$^{\Delta R}$ cells resulting from removal of floxed exons 20 and 21.

(C) Expression of spliced *Xbp1* over a time course following *Ca* infection.

(D) Expression of spliced *Xbp1* at 4 h post-infection (hpi) with the indicated isolates.

(E) Expression of spliced *Xbp1* at 4 h following *Ca* infection or LPS treatment of WT or CARD9 KO iBMDM.

(F) Expression of spliced *Xbp1* at 4 h following *Ca* infection and depleted zymosan (d-zymosan) or LPS treatment of WT or IRE1$^{\Delta R}$ iBMDM.

(G) Expression of spliced *Xbp1* at 4 h following *Ca* infection, LPS treatment, or d-zymosan treatment of WT or TLR2/4/9 KO iBMDM.

(H) Expression of spliced *Xbp1* at 4 h following *Ca* infection or LPS treatment of two pairs of clonal iBMDM (WT or TRAF6 KO). Closed symbols are data from WT-1 and KO-1; open symbols are data from WT-2 and KO-2. Data are representative of 3–4 individual experiments.

Graphs show the mean ± SEM of biological replicates (C–H). For all experiments, *Ca* MOI = 1, LPS treatment = 100 ng/mL, d-zymosan = 100 μg/mL, thapsigargin = 5 μM. Statistical analysis details are in STAR Methods.

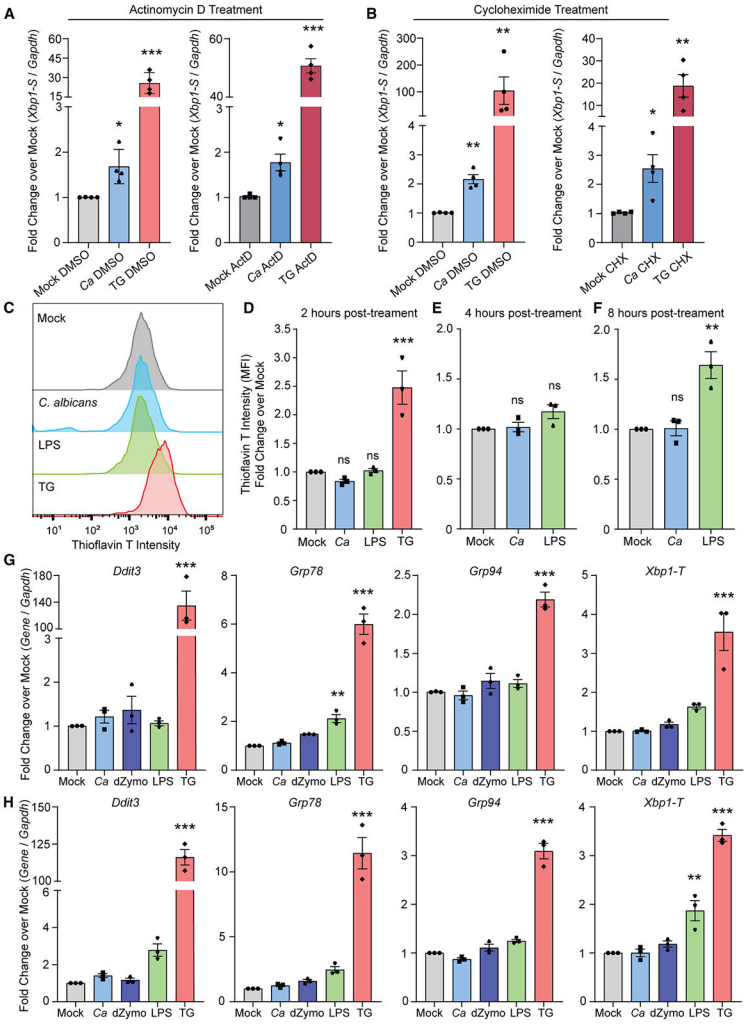

Figure 2. PRR-mediated activation of IRE1α occurs independently of misfolded protein stress

(A and B) Expression of spliced *Xbp1* following *C. albicans* infection of iBMDM or treatment with thapsigargin (TG) as a control, compared to mock treatment. Actinomycin D (ActD; 20 μM) was used to inhibit new transcription during treatments (A), and cycloheximide (CHX; 10 μM) was used to inhibit translation during treatments (B). Relative fold changes were measured over matched mock samples.

(C) Representative graphs showing fluorescence intensity of Thioflavin T (ThT) measured by flow cytometry to quantify protein misfolding in iBMDM following infection by *C. albicans* or treatment with LPS or thapsigargin as a positive control at 2 h.

(D–F) Quantification of ThT fluorescence intensity at 2 h (D), 4 h (E), or 8 h (F) post-indicated treatment, shown as fold change over mock.

(G and H) Expression of UPR-responsive genes at 4 h (G) or 6 h (H) following *C. albicans* infection and d-zymosan, LPS, or thapsigargin treatment.

Statistical analysis details are in STAR Methods. For all experiments, *Ca* MOI = 1, LPS treatment = 100 ng/mL, d-zymosan = 100 μg/mL, thapsigargin = 5 μM.

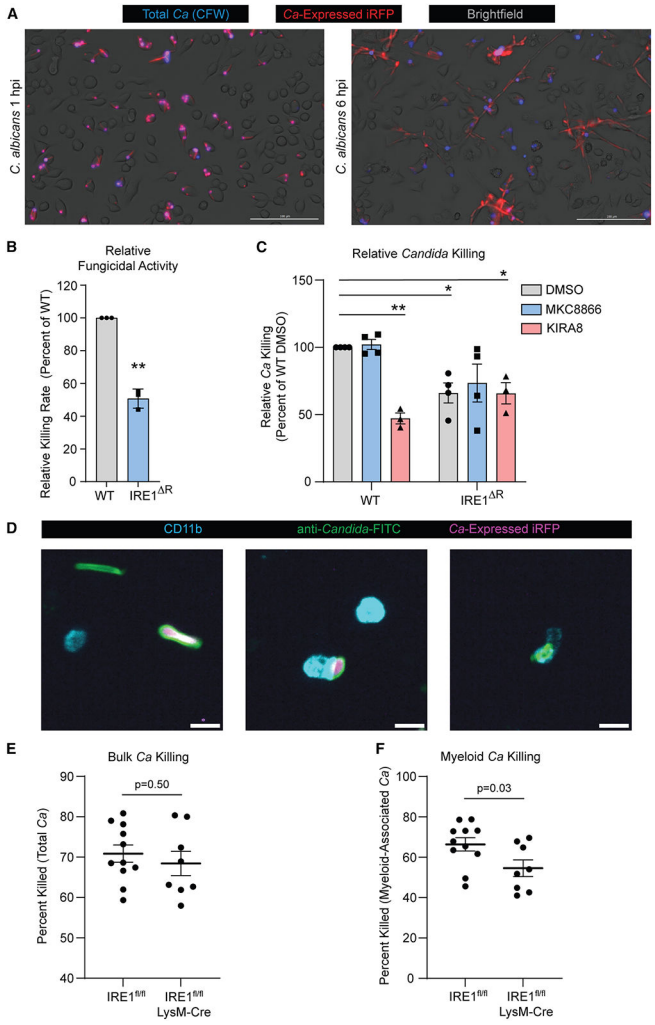

Figure 3. IRE1α promotes macrophage fungicidal activity

(A) Representative widefield micrographs of live (CFW^{+} iRFP^{+}) and killed (CFW^{+} iRFP^{-}) intracellular *C. albicans* within IRE1 WT iBMDM at 1 hpi (left) and 6 hpi (right). Scale bar, 100 μm.

(B) Quantification of three independent *C. albicans*-killing experiments.

(C) Quantification of relative *C. albicans* killing 6 hpi in IRE1 WT or IRE1$^{\Delta R}$ iBMDM treated with pharmacological inhibitors of IRE1α targeting RNase domain (MKC8866; 10 μM), kinase domain (KIRA8; 1 μM), or control DMSO treatment; relative killing is calculated as the percentage of IRE1 WT DMSO treatment.

(D) Representative micrographs of *C. albicans* in dissociated kidney cells showing total *C. albicans* (anti-*Candida*-fluorescein isothiocyanate^{+} [FITC^{+}]) in green, live *C. albicans* in green and magenta (anti-*Candida*-FITC^{+} *C. albicans*-expressed iRFP^{+}), and CD11b^{+} cells in blue to identify host leukocytes. Images show non-myeloid-associated live and dead *C. albicans* (left), myeloid-associated live *C. albicans* (center), and myeloid-associated killed *C. albicans* (right). Scale bar, 10 μm.

(E and F) Percentage of *C. albicans* killed was quantified in the kidney tissue (E) or specifically in myeloid cells (F).

Graphs show the mean ± SEM of 3–4 biological replicates (B and C), or of data from individual mice (E and F). Statistical analysis details are in STAR Methods.

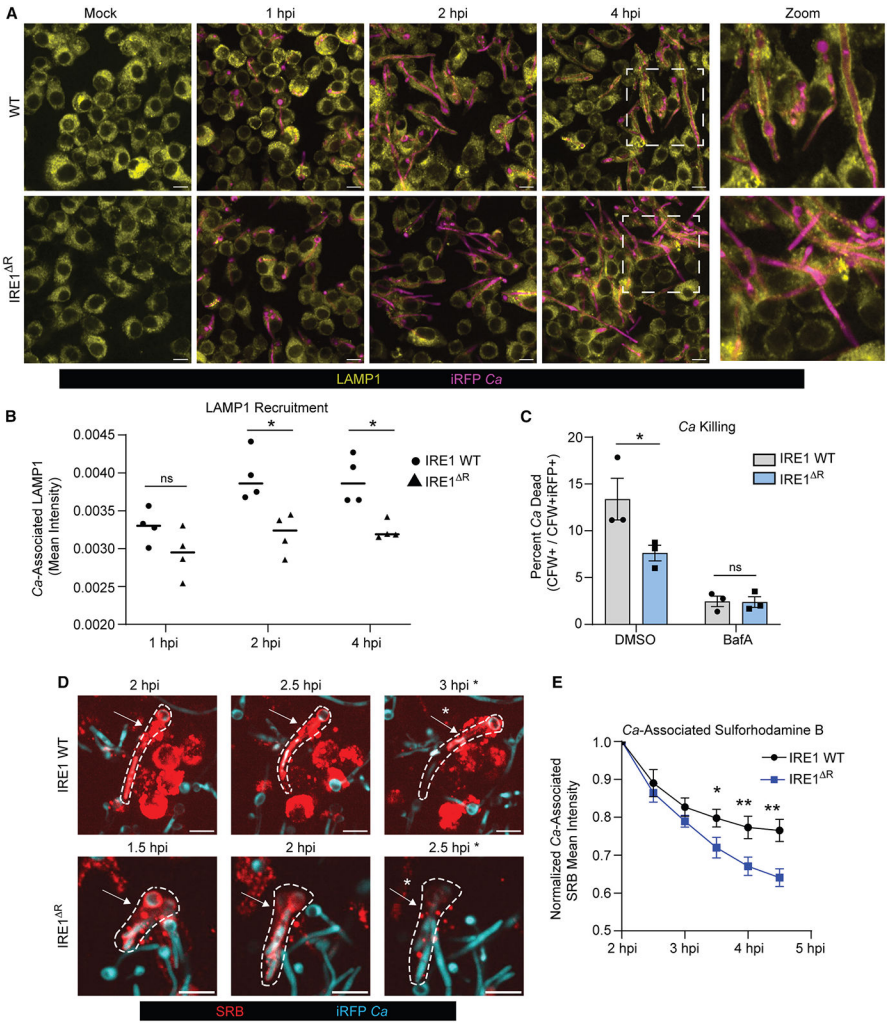

Figure 4. IRE1α promotes phagosome maturation during *C. albicans* infection

(A) Representative images showing LAMP1 (yellow) recruitment to phagosomes containing iRFP-expressing *C. albicans* (magenta) in IRE1 WT or IRE1$^{\Delta R}$ iBMDM at indicated times post-infection.

(B) Quantification of LAMP1 recruitment to phagosomes containing *C. albicans* in IRE1 WT or IRE1$^{\Delta R}$ iBMDM, as measured by LAMP1 mean fluorescence intensity associated with *C. albicans*-expressed iRFP.

(C) Quantification of *C. albicans* killing in IRE1 WT and IRE1$^{\Delta R}$ macrophages treated with BafA or DMSO control.

(D) Representative images of SRB recruitment to the phagosome containing *C. albicans*, indicated by white arrows, and loss of SRB association following phagosomal rupture, indicated by white asterisk. Scale bar, 10 μm.

(E) Quantification of three independent experiments measuring loss of SRB from *C. albicans* over time in IRE1 WT or IRE1$^{\Delta R}$ iBMDM.

Values are the mean ± SEM of 3–4 biological replicates. Statistical analysis details are in STAR Methods.

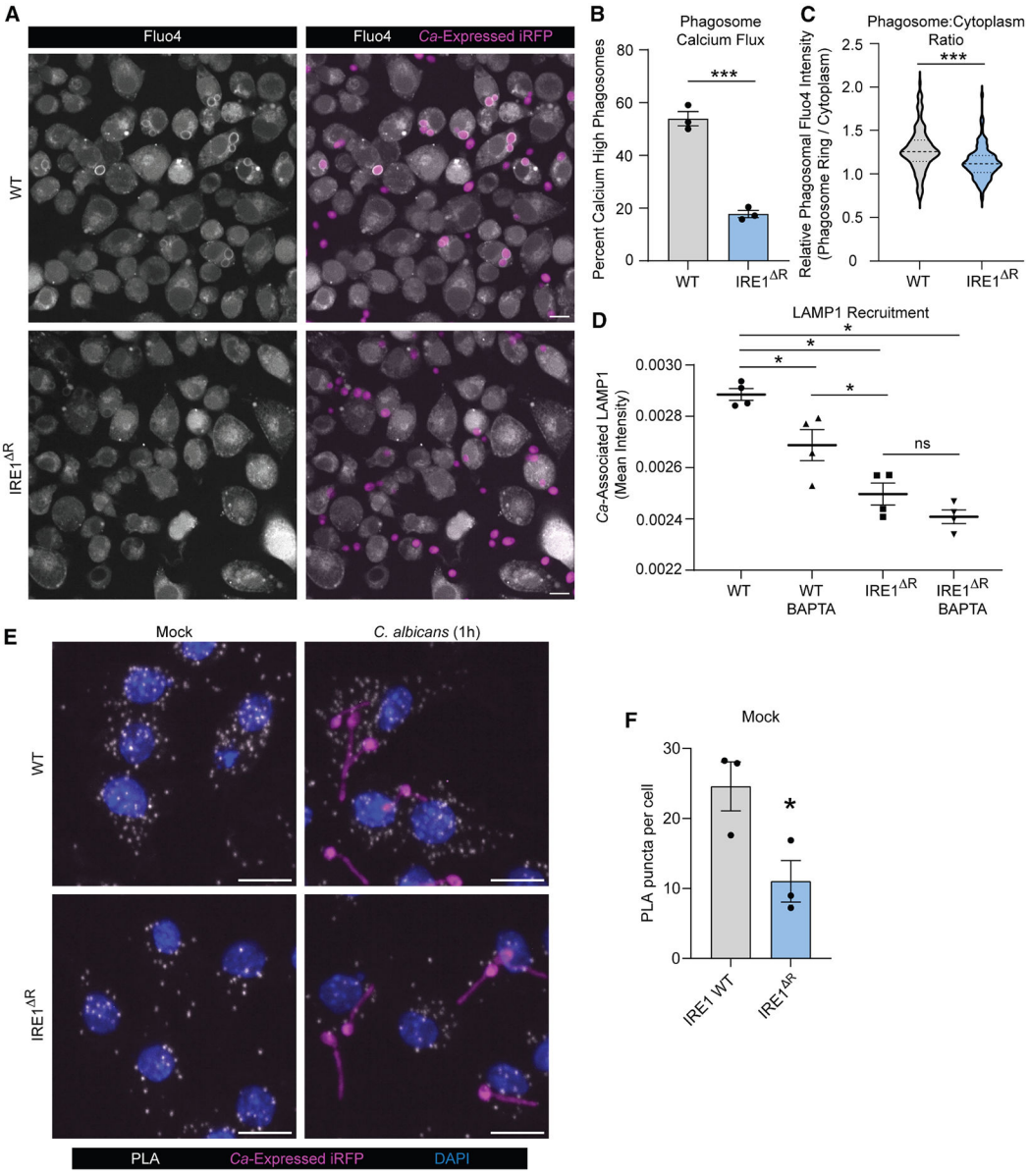

Figure 5. IRE1α promotes phagosomal calcium flux and contact sites between the ER and endosomal network

(A) Representative micrographs of WT or IRE1$^{\Delta R}$ iBMDM following phagocytosis of *C. albicans* (20 min post-infection; MOI 2) showing early cellular calcium flux, and influx of calcium specifically in the phagosome following phagocytosis of *C. albicans*. Scale bar, 10 μm.

(B) Quantification of calcium-high phagosomes, defined by a 1.25-fold increase of the mean fluorescence intensity of the cell (20 min post-infection; MOI 2).

(C) Violin plot of the ratio of phagosomal to cytosolic mean fluorescence intensity of Fluo4 (20 min post-infection; MOI 2).

(D) Quantification of LAMP1 recruitment to phagosomes containing *C. albicans* in IRE1 WT or IRE1$^{\Delta R}$ iBMDM with or without treatment of BAPTA-AM (calcium chelator), as

measured by LAMP1 mean fluorescence intensity associated with *C. albicans*-expressed iRFP.

(E) Representative confocal micrographs of PLA puncta representing sites of proximity between the ER and early endosomes/phagosomes at resting state (mock) or during *C. albicans* infection. Scale bar, 10 μm.

(F) Quantification of PLA puncta in IRE1 WT or IRE1$^{\Delta R}$ iBMDM at resting state (mock). Values are the mean ± SEM from 3 to 4 biological replicates, as indicated by data points. Statistical analysis details are in STAR Methods.

KEY RESOURCES TABLE

REAGENT or RESOURCE	SOURCE	IDENTIFIER
Antibodies		
Rabbit monoclonal anti-IRE1α	Cell Signaling	Cat#3924; RRID:AB_823545
Rabbit polyclonal anti-XBP1	Abcam	Cat#ab37152; RRID:AB_778939
Rabbit polyclonal anti-CARD9	Cell Signaling	Cat#12283; RRID:AB_2797869
Mouse monoclonal anti-ACTIN	ThermoFisher	Cat#MA5-11869; RRID:AB_11004139
Rabbit monoclonal anti-TRAF6	Abcam	Cat#ab40675; RRID:AB_778573
Rabbit polyclonal anti-K48-linkage specific polyubiquitin	Cell Signaling	Cat#4289; RRID:AB_10557239
Rabbit monoclonal anti-ATF6	Cell Signaling	Cat#65880; RRID:AB_2799696
Rabbit polyclonal anti-phospho-eIF2α Ser51	Cell Signaling	Cat#9721; RRID:AB_330951
Mouse monoclonal anti- eIF2α	Cell Signaling	Cat#2103; RRID:AB_836874
Rabbit monoclonal anti-ATF4	Cell Signaling	Cat#11815; RRID:AB_2616025
Rabbit polyclonal anti-Candida albicans-FITC	LSBio	Cat#LS-C103355
Rat monoclonal anti-LAMP1	DSHB	Cat#1D4B; RRID:AB_2134500
Mouse monoclonal anti-EEA1	ThermoFisher	Cat#MA5-31575
Rabbit monoclonal anti-KDEL	Abcam	Cat#ab176333; RRID:AB_2819147
Rat monoclonal anti-CD11b, BV421-conjugated	Biolegend	Cat#414-0112-82
Bacterial and virus strains		
MRSA-mCherry	Boles et al. 2008[73]	N/A
Methicillin-resistant *Staphyloccocus aureus* USA300 LAC harboring p*SarA*-mCherry plasmid		
Chemicals, peptides, and recombinant proteins		
Thioflavin T	Cayman Chemical	Cat#32553; CAS Number 2390-54-7
TRIzol reagent	Thermo Fisher	Cat#15596018
Turbo DNase I	Thermo Fisher	Cat#AM2238
Paraformaldehyde	Electron Microscopy Services	Cat#15700
Calcofluor white	Sigma-Aldrich	Cat#18909
Bovine serum albumin	Thermo Fisher	Cat#BP9706-100
Sulforhodamine B	Sigma-Aldrich	Cat#230162; CAS Number 3520-42-1
Critical commercial assays		
Lookout Mycoplasma PCR Detection Kit	Sigma-Aldrich	Cat#MP0035
iScript cDNA synthesis kit	BioRad	Cat# 1708891
PowerUP SYBR Green qPCR master mix	Thermo Fisher	Cat# A25742
Fluo-4 Calcium Imaging Kit	Invitrogen	Cat#F10489
LysoSensor Yellow/Blue DND-160	Thermo Fisher	Cat#L7545
LysoTracker Deep Red	Invitrogen	Cat#L12492
Duolink *In Situ* PLA Kit	Sigma-Aldrich	Cat#DUO92008 Cat#DUO92002 Cat#DUO92004
Fluorospheres	Thermo Fisher	Cat#F8801

REAGENT or RESOURCE	SOURCE	IDENTIFIER
Deposited data		
Raw and processed RNA-seq data	This paper	GEO: GSE244303
Experimental models: Cell lines		
IRE1 WT and IRE1$^{\Delta R}$ immortalized bone marrow-derived macrophages (iBMDM) from *Mus musculus* C57BL/6J	This paper	N/A
WT primary bone marrow-derived macrophages (BMDM) from *Mus musculus* C57BL/6J	This paper	N/A
CARD9 knockout and WT iBMDM from *Mus musculus* C57BL/6J	Dr. Stuart Levitz	N/A
TLR2/4/9 knockout and WT iBMDM from *Mus musculus* C57BL/6J	Dr. Tod Merkel	N/A
TRAF6 knockout and TRAF6 WT iBMDM from *Mus musculus* C57BL/6J	This paper	N/A
Experimental models: Organisms/strains		
Mouse: *Mus musculus* C57BL/6J	The Jackson Laboratory	RRID:IMSR_JAX:000664
Mouse: IRE1 flox/flox	Iwawaki et al. 2009[38]	N/A
Mouse: IRE1 flox/flox X LysM^{Cre}	This paper	N/A
Candida albicans reference strain SC5314	O'Meara et al. 2015[33]	N/A
Candida albicans SC5314 expressing iRFP driven by pENO1 promoter	Ost et al. 2021[74]	N/A
Oligonucleotides		
Cre-GFP Forward primer: TAAAGCG GCCGCTATGGCCAATTTACTGACCG	This paper	N/A
Cre-GFP Reverse primer: CTCTAGAC TCGAGTTAACTTACTTGTACAGCTCGTCCA	This paper	N/A
Xbp1-S RT-qPCR Forward primer: GC TGAGTCCGCAGCAGGT	This paper	N/A
Xbp1-S RT-qPCR Reverse primer: CAGGGTCCAACTTGTCCAGAAT	This paper	N/A
Gapdh RT-qPCR Forward primer: CATCACTGCCACCCAGAAGACTG	This paper	N/A
Gapdh RT-qPCR Reverse primer: ATGCCAGTGAGCTTCCCGTTCAG	This paper	N/A
Ddit3 RT-qPCR Forward primer: GGAGGTCCTGTCCTCAGATGAA	This paper	N/A
Ddit3 RT-qPCR Reverse primer: GCTCCTCTGTCAGCCAAGCTAG	This paper	N/A
Grp78 RT-qPCR Forward primer: GTGTTCAAGAACGGCCGCGTG	This paper	N/A
Grp78 RT-qPCR Reverse primer: GTTTGCCCACCTCCAATATCAAC	This paper	N/A
Grp94 RT-qPCR Forward primer: GTTTCCCGTGAGACTCTTCAGC	This paper	N/A
Grp94 RT-qPCR Reverse primer: ATTCGTGCCGAACTCCTTCCAG	This paper	N/A
Xbp1-T RT-qPCR Forward primer: TGAAAAACAGAGTAGCAGCGCAGA	This paper	N/A
Xbp1-T RT-qPCR Reverse primer: CCCAAGCGTGTTCTTAACTC	This paper	N/A
Recombinant DNA		
pLEX-FLAG-Cre-GFP	This paper	N/A
pLEX-FLAG-GFP	Dr. Stacy Horner	N/A
psPAX2	Dr. Stacy Horner	RRID:Addgene_12260
pMD2.G	Dr. Stacy Horner	RRID:Addgene_12259
Software and algorithms		
CellProfiler Pipelines S1-S9	Stirling et al. 2021[75]	https://cellprofiler.org/
Fiji/ImageJ	Schindelin et al. 2012[76]	https://imagej.net/software/fiji/

REAGENT or RESOURCE	SOURCE	IDENTIFIER
Cellular Calcium Flux Analysis software	This paper	https://github.com/EinarOlafsson/spacr
Cellpose	Stringer et al. 2021[77]	https://www.cellpose.org/
ImageStudio	LICORbio	https://www.licorbio.com/image-studio
Galaxy	N/A	Usegalaxy.org
Cutadapt	Martin et al. 2011[78]	https://cutadapt.readthedocs.io/en/stable/
Kallisto	Bray et al. 2016[79]	https://pachterlab.github.io/kallisto/
DEseq2	Love et al. 2014[80]	https://bioconductor.org/packages/release/bioc/html/DESeq2.html